A critical review on biochar-based engineered hierarchical porous carbon for capacitive charge storage

Published in: *Renewable and Sustainable Energy Reviews*

Citation for published version: Cuong, D.V., Matsagar, B.M., Lee, M., Hossain, M.S.A., Yamauchi, Y., Vithanage, M., Sarkar, B., Ok, Y.S. Wu, K.C.-W., Hou, C.H., (2021) A critical review on biochar-based engineered hierarchical porous carbon for capacitive charge storage. Renewable and Sustainable Energy Reviews. 145: 111029. doi: 10.1016/j.rser.2021.111029.

Document version: Accepted peer-reviewed version.

A critical review on biochar-based engineered hierarchical porous carbon for capacitive charge storage

Dinh Viet Cuong,[a,b] Babasaheb M. Matsagar,[c] Mengshan Lee,[d] Md. Shahriar A. Hossain,[e] Yusuke Yamauchi,[e] Meththika Vithanage,[f] Binoy Sarkar [g], Yong Sik Ok,[h,*] Kevin C.-W. Wu,[c,*] and Chia-Hung Hou[a,*]

[a]*Graduate Institute of Environmental Engineering, National Taiwan University, Taipei 10618, Taiwan*

[b]*Faculty of Environmental Engineering, National University of Civil Engineering, Hanoi 100000, Vietnam*

[c]*Department of Chemical Engineering, National Taiwan University, No. 1, Sec. 4, Roosevelt Road, Taipei 10617, Taiwan*

[d]*Department of Safety, Health and Environmental Engineering, National Kaohsiung University of Science and Technology, Kaohsiung 824, Taiwan*

[e]*School of Chemical Engineering, School of Mechanical & Mining Engineering, Australian Institute for Bioengineering and Nanotechnology (AIBN), The University of Queensland, Brisbane, QLD 4072, Australia*

[f]*Ecsophere Resilience Research Centre, Faculty of Applied Sciences, University of Sri Jayewardenepura, Nugegoda 10250, Sri Lanka*

[g]*Lancaster Environment Centre, Lancaster University, Lancaster, LA1 4YQ, United Kingdom*

[h]*Korea Biochar Research Center, APRU Sustainable Waste Management & Division of Environmental Science and Ecological Engineering, Korea University, Seoul, Republic of Korea*

***Corresponding author: yongsikok@korea.ac.kr (Yong Sik Ok), kevinwu@ntu.edu.tw (K.C-W. Wu) and chiahunghou@ntu.edu.tw (C.-H.Hou).**

Graphical abstract

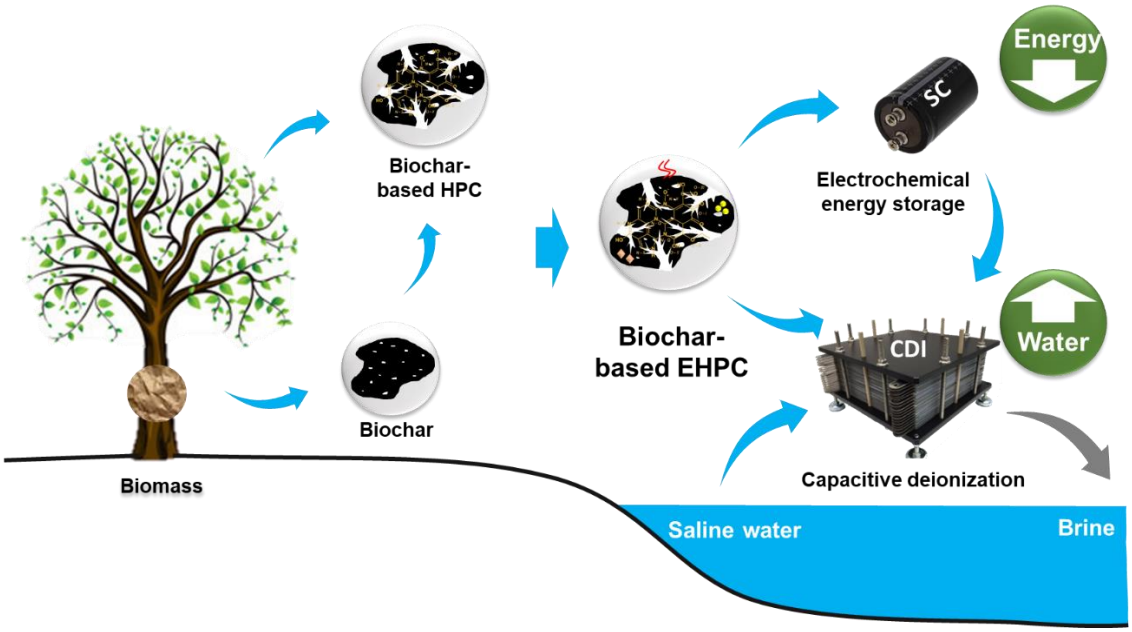

Abstract

Hierarchical porous carbon (HPC) has attracted increasing research interest for energy and environmental applications. HPC is conventionally fabricated by activated carbon, which potentially causes hidden environmental burdens. To overcome this issue, biochar, a promising renewable precursor, offers an attractive raw material substitute and has already been explored for the preparation of low-cost HPC. Recent studies have demonstrated that HPC exhibited great applications in capacitive energy storage, owning to its easily tuned physicochemical and electrochemical properties. Besides, biochar-based HPC with a three-dimensional (3D) interconnected controllable pore structure, high specific surface area (SSA), and pore volume (PV) can provide smaller resistance and shorter diffusion pathways for the transport of ions. Importantly, most recent research efforts have been made on the synthesis of biochar-based engineered hierarchical porous carbons (EHPCs) from biomass/biochar or developed from the HPC. A templating technique, heteroatom, and metal oxides doping have been applied to develop the biochar-based EHPC to improve 3D pore structure or/and expose abundant active sites and subsequently enhance the capacitive charge storage performance. In this review, recent advances in the applications of biochar-based HPC or EHPC for capacitive charge storage, e.g., capacitive deionization (CDI) and a supercapacitor (SC) are summarized and discussed. This review concludes with several perspectives to provide possible future research directions for the preparation and applications of biochar-based EHPC for capacitive charge storage.

Keywords: Biomass, Biochar, Engineered hierarchical porous carbon, Capacitive charge, Electrochemical energy storage.

Contents

1. Introduction

Biomass is currently attracting significant attention as an alternative precursor to fossil-based feedstock in the production of carbon materials; because biomass is a naturally renewable, abundant, low-cost, easily accessible, and environmentally friendly resource [1-3]. Consequently, the development of sustainable carbon materials from biomass is a promising solution, not only because it has the potential to replace conventional carbons but also its ability to contribute to solid waste management in large quantities from the manufacturing and agriculture sectors. In recent years, various forms of biomass such as lignin, carbohydrates, cellulose, chitin, and proteins have been widely utilized to prepare carbon materials [4].

Biochar is typically generated via thermal decomposition of biomass at a moderate temperature (350-700 °C) without oxygen or with a limited oxygen supply [5]. It is regarded as an emerging substitute for conventional carbons to reduce its associated environmental impacts. However, biochar in its raw form may have a limited adsorption performance, due to its poor porous nature and low activity [6, 7]. Hierarchical porous carbon (HPC), an improved form of porous carbon, holds the merits of high specific surface area (SSA), large pore volume (PV), and well-tailored pore dimensions. Recently, biochar is extensively used in the preparation of HPC due to its renewable and environmentally friendly nature compared with other carbonaceous precursors [1, 8-10].

The unique three-dimensional (3D) interconnected porous structure of biochar-based HPC in terms of macropores (>50 nm), mesopores (2–50 nm), and micropores (<2 nm) (Fig. 1) play a significant role in its improved efficiency for various applications, including capacitive charge storage, environmental remediation, and electrochemical deionization [11, 12]. This review is focused on the design, preparation

and applications of engineered biochar-derived HPC for capacitive charge storage. More specifically, the hierarchical porous structure of biochar-based HPC can offer a large interface with electrolytes for charge storage reactions. For instance, mesopores and macropores contribute to the rapid transport of ions and molecules, respectively, through channels to micropores, which facilitate rapid mass transfer kinetics and low mass transfer resistance [13, 14]. The matter diffusion distance inside pores can be minimized by the buffering reservoir in the mesopores, which supports a large accessible surface area and low resistance transport pathway for ion/molecule adsorption. Micropores, on the other hand, provide plentiful active sites that are beneficial for enhancing ions/molecules separation and electron capacity [15, 16].

Biochar-based engineered HPC (EHPC) can be synthesized from biomass/biochar or developed from biochar-based HPC through some technical strategies to enhance the capacitive charge storage. The development of pores in biochar-based EHPC can be performed by a templating method [17]. In addition, heteroatom doping (e.g., N, O, S, and P) on the surface of biochar-based EHPC is another approach to improve electrochemical properties [18, 19]. The involvement of surface functional groups on biochar-based EHPC can provide abundant reactions or interaction sites for surface or interface-related processes such as the formation of lithium-oxygen (Li-O) interaction in batteries, and pseudo-Faradaic reactions in supercapacitors (SCs). Oxygen functional groups (i.e, quinone type (O-I), phenol/ether groups (O-II), and chemisorbed oxygen (COOH carboxylic groups)/water (O-III)) are mostly available on the surface of biochar-based EHPC, while N functionalities, including pyrrolic (N-5), pyridinic (N-6), quaternary N (N-Q), and pyridine-N-oxide (N-X) observed on N-doped biochar-based HPC and EHPC [20-23] (Fig. 1). Moreover, the development of biomass-based HPC using impregnation of metal oxides, such as

MnO_2, $CoFe_2O_4$ was reported with the enhanced electrochemical performance [24, 25]. These techniques play important roles in achieving high performance in biochar-based EHPC applications.

The increasing interest of the scientific community in biochar-based HPCs between 2009 and 2019 (according to ISI Web of Science™ verified in March 2020), as shown in Fig. 2. Recent studies have demonstrated the applications of biochar-based HPC for electrosorption and electrochemical energy storage, e.g., lithium-sulfur (Li-S) batteries [26], Li-ion batteries [27], dye-sensitized solar cells [14] and supercapacitors (SCs) [28, 29] has shown a great future potential [30]. Besides, biochar-based HPC is efficiently utilized for the removal of heavy metals [31-34] and organic compounds [35-37], as well as for CO_2 adsorption [38].

Biomass is an inexpensive, easily available promising renewable source for the synthesis of functional carbon materials. Hence the utilization of biomass/biochar-derived EHPCs can promote the future research and applications of HPCs. Besides, the incorporation of heteroatoms can enhance future research outcomes for energy storage applications, including batteries, fuel cells, and supercapacitors; because the incorporation of heteroatom enhances the performance of the energy storage applications [39]. Some biomass contains nitrogen (shrimp shell and soybean residue) that can help to directly convert biomass into N-doped hierarchical porous carbon without using additional nitrogen precursor. The increase in renewable energy contribution is necessary for our future energy security and increasing energy efficiencies and demand. Consequently, focusing on biomass/biochar-derived EHPCs synthesis and its utilization for various applications is crucial. Considering the sustainability and environmental benefits of biochar-based EHPCs and the scope for various applications, there is a lack of comprehensive review on the fabrication and

applications of biochar-based EHPCs. This work reviews various preparation methods (e.g., hard-template, self-template, or non-template) for biochar-based HPC with each step (e.g., carbonization, leaching, and activation). Moreover, modification and advancement of the biochar-based EHPC to enhance its physicochemical and electrochemical properties are introduced. Finally, future research perspectives and conclusions are presented in detail.

2. Preparation of biochar-based HPC and EHPC

Carbonization is a thermal treatment process, which is performed under a limited or anti-oxygen atmosphere to convert organic matters such as biomass into a stable porous carbon, the biochar. The carbonization of biomass would undergo polymer reduction and fragmentation stages [40, 41], which involved the release of O_2, CO, CO_2, H_2, and H_2O as well as condensable volatiles in the course of obtaining biochar [42]. Subsequently, large macropores (2 to 10 μm) may be formed by residual gaps from the removal of organic constituents. Carbonization methods such as pyrolysis, gasification, HTC, and torrefaction can be employed in the preparation of biochar from different biomass sources (e.g., agriculture, bioenergy crop, forest residue, and sewage sludge) [43]. In addition, the carbonization methods can be controlled by varying temperature, heating rate, and heating time to achieve biochar with desired physicochemical properties and higher yields.

The synthesis of biochar-based HPC and biochar-based EHPC uses many common methods; however, in the case of biochar-based EHPC, the synthesis conditions are well optimized to tune the physicochemical properties of the EHPC for desired capacitive charge storage applications. Biochar-based EHPC is typically fabricated by either templating or non-templating methods. In the non-templating

147 method, it is difficult to control the formation and growth of hierarchical pore
148 architecture in terms of the shape and size distribution of the particles, while alkali
149 activation was proven to reconstruct or improve its hierarchical pore network [44]. For
150 the templating method, the 3D pore structure is developed and controlled using porous
151 inorganic solid-state hard-templates as a frame structure and amphiphilic block
152 copolymers soft-templates as structure-directing agents [45]. The hard-templates
153 showed higher control of the product. The major challenge for the synthesis of EHPC
154 by hard-templating is the synthesis of porous inorganic materials as hard-templates such
155 as silica spheres, mesoporous silica, or polymer spheres, which can be tedious, time-
156 consuming, and can be expensive. Besides, the hard-template removal process may
157 introduce additional use of highly corrosive chemicals (HF or NaOH), which is
158 environmentally unfriendly. Hence, the optimization of the materials for the preparation
159 of the EHPC should be investigated to avoid the use of corrosive chemicals. In contrast,
160 the removal of soft templates is a facile process. However, the morphology of the
161 desired product is difficult to control. Most of the already explored soft-templates are
162 based on rather expensive and non-renewable surfactants and block-copolymers [44].
163

164 ### 2.1. Developing 3D interconnected pore system inside biochar-based HPC

165 Recent studies on the preparation of biochar-based HPC and EHPC are
166 presented in Table 1. Biochar-based HPC is commonly prepared by the template-free
167 method, including carbonization and/or activation, e.g., one-step pyrolysis [34], two-
168 step pyrolysis [46], pyrolysis and hydrothermal carbonization (HTC) [31], pyrolysis
169 and activation [47], HTC, activation [48], one-step chemical activation [49], and one-
170 step physical activation [50]. Generally, the preparation process of biochar-based HPC
171 may include the following steps (Fig. 3): (1) carbonization of biomass to prepare

biochar; (2) pretreatment to remove the templates used in templating methods; and (3) activation to develop the hierarchical porous structure. The carbonization of biomass would undergo polymer reduction and fragmentation stages [40, 41], which involved the release of O_2, CO, CO_2, H_2, and H_2O and condensable volatiles in the course of obtaining biochar [42]. Subsequently, large macropores (2 to 10 μm) may be formed by residual gaps from the removal of organic constituents.

2.1.1. Pretreatment of biochar

The presence of major and minor elements in biomass might impede porosity development. Therefore, pretreatment is typically applied before the activation step to remove metals and other impurities. After the pretreatment process, many mesopores and micropores can be generated. Acid washing (e.g., HCl, HF, H_2SO_4, and HNO_3) or base leaching is a common means for biochar pretreatments. Especially, the acid or base leaching step is typically applied to eliminate the natural inorganic template in biomass (Table 1). This step increases the contact between the carbon matrix and activation agent, as well as further enhance the efficiency of the activation process and porous structure development.

2.1.2. Activation of biochar

Activation of biochar can be performed by physical, chemical, or physicochemical processes with different activation agents and reaction parameters (e.g., activation temperature (350-1000 ºC) and activation time (0.5-10 h)), as shown in Fig. 4. Depending on the activation method, i.e., physical, chemical and physicochemical methods, the plausible pore formation and distribution are varied.

Physical activation

Physical activation, a thermal process that biochar partially gasified by an

oxidant atmosphere (usually CO_2, steam, oxygen, or their mixtures), the disorganized material is removed and subsequently increase in porosity [51]. Physical activation is an environmentally friendly method because it uses inexpensive activating agents and no secondary waste generation, and there are no requirements for specialized equipment or material. Nonetheless, it requires a long activation time (0.5 to 10 h), leading to large energy consumption (as shown in Table 1). Additionally, physical activation provides HPC with moderate SSA (*ca.* 1000 m^2 g^{-1}) and PV (Table 1). Micropores are normally dominant in biochar-based HPC and may range from 60-80 % of total PV [50, 52, 53].

The combination of one-step or two-step carbonization and physical activation using a gasification agent is a relatively common and simple approach to synthesize biochar-based EHPC from biomass. For instance, the approach may only involve the utilization of O_2 as the activation agent. Many researchers also agreed that CO_2 is a superior physical activation agent due to it is less reactivity at high temperatures, resulting in favorable controllability of porous structure [1, 17, 50]. Physical activation normally applies at a temperature range between 700 and 1000 °C in steam or CO_2, and lower temperatures in the air [54]. Carbon atoms with higher activity are removed during physical activation via reactions shown in Eq. (1) and Eq. (2), which leads to the development of porosity, the hierarchical porous structure, and an increase in SSA. Besides, the nature of the pore and yield of physically activated biochar is strongly dependent on the heating conditions. For example, the microwave heating with CO_2 activation exhibited higher biochar yield compared to conventional heating, however, the insignificant effect for biochar yield was noted for steam-activation [55]. Conversely, the PV and SSA were doubled for steam-activated biochar, when combined with microwave heating instead of conventional heating [56].

$$C\ (s) + CO_2\ (g) = 2CO\ (g) \quad (1)$$

$$C\ (s) + H_2O\ (g) = CO\ (g) + H_2\ (g) \quad (2)$$

Chemical activation

Chemical activation of biochar is commonly done by impregnating with chemical activation agents, such as alkali hydroxide (e.g., KOH and NaOH), carbonates (K_2CO_3, and Na_2CO_3), zinc chloride ($ZnCl_2$) and some acids (e.g., H_3PO_4 and H_2SO_4), followed by heating in an inert atmosphere (e.g., N_2 and Ar) at high temperature [57, 58]. As organized in Table 1, chemical activation requires a shorter activation time (0.5 to 2 h) and lower temperature, leading to smaller energy consumption than physical activation. In addition, KOH is the most common and effective activation agent in the preparation of biochar-based HPC, which can produce biochar-based EHPCs with ultrahigh SSA of over 3000 $m^2\ g^{-1}$ [59]. During KOH activation, pores are formed by a collective effect of various factors. Firstly, biochar etching will happen via reactions shown in Eqs. (3), (6), and (7), which subsequently escape CO and H_2 gaseous products from biochar resulting in the formation of macropores. Secondly, the CO_2 and H_2O formed in situ during the carbonization can show additional physical activation. Then the development of the hierarchical porous structure with abundant micropores and mesopores of biochar-based HPC using KOH chemical activation is attributed to the chemical reactions, as shown in Eqs. (3)-(8).

$$6KOH\ (s) + 2C\ (s) \longrightarrow 2K\ (s) + 3H_2\ (g) + 2K_2CO_3\ (s) \quad (3)$$

$$K_2CO_3\ (s) \longrightarrow K_2O\ (s) + CO_2\ (g) \quad (4)$$

$$CO_2 + C\ (s) \longrightarrow 2CO\ (g) \quad (5)$$

$$K_2CO_3\ (s) + 2C\ (s) \longrightarrow 2K\ (s) + 3CO\ (g) \quad (6)$$

$$K_2O\ (s) + C\ (s) \longrightarrow 2K\ (s) + CO\ (g) \quad (7)$$

$$2KHCO_3 \longrightarrow K_2CO_3 + CO_2 + H_2O \quad (8)$$

Compared to physical activation, chemical activation showed significantly larger SSA, higher pore volume and mesoporosity because the pore-forming mechanism is carried out through many chemical reactions. For instance, Wei et al. synthesized HPC from yeast by chemical activation using KOH at 850 ºC for 1 h. It was found that the EHPC contained ultra-high SSA (3808 $m^2\ g^{-1}$) and pore volume (2.20 $m^3\ g^{-1}$) [60]. One has to note that the activation agents can cause serious corrosion to the reactor, which requires rigorous washing to eliminate the excessive residue of activating reagents that adversely affect the environment [61].

Physicochemical activation

Physicochemical activation is a combined process of physical and chemical activation. It can be performed by chemical impregnation onto biochar or biomass by activating agents similar to the chemical activation process, followed by thermal treatment under an oxidizing atmosphere (e.g., CO_2, steam, or O_2) at a high temperature. Physicochemical activation should be applied when the HPC requires additional pore formation and the development of unique textural properties (e.g., high ratio of mesoporosity). However, physicochemical activation is a more complex process and requires higher investment (e.g., reagents and auxiliary equipment) than a single activation method.

The comparison of SSA and mesoporosity of biochar-based HPCs derived from various biomass precursors is shown in Fig. 5. It should be noted that mesopores are particularly advantageous for applications of capacitive charge storage. On the other hand, narrow micropores are less effective for capacitive charge storage [62, 63]. The

classification of these biochar-based HPC presents 4 groups based on the SSA and mesoporosity. Group I is assigned to HPCs with SSA below 2000 $m^2 g^{-1}$ and less than 40% mesoporosity. For example, biochar-derived HPC from corn husk, natural basswood, and auricularia fall in this group. Group II includes HPCs derived from wood powder, *Leucaena leucocephala* wood, soybean milk, and fishbone in which the SSA is lower than 2000 $m^2 g^{-1}$ and mesoporosity is higher than 40%. Finally, Group III (e.g., HPCs derived from chestnut, yeast, soybean root, and bovine bone) and IV (e.g., HPCs derived from *enteromorpha prolifera*, silkworm cocoon, and shrimp shell) involve HPCs that exhibited an ultra-high SSA. However, the mesoporosity of biochar-based HPCs in Group III and IV is lower than 40% and greater than 40%, respectively. Notably, rice husk biochar-based HPC was prepared through physicochemical activation using KOH combined with CO_2 resulted in high SSA (2330 $m^2 g^{-1}$) and mesoporosity (81%) [17], compared to other rice husk biochar-based HPC synthesized by chemical activation only [13, 14, 26].

2.2. Design of biochar-based EHPC

Generally, applying a design step to improve the quality as well as the application performance of EHPC. It can be applied in conjunction with the activation step or as a post-treatment step. The enhancement of the porosity of biochar-based EHPC is beneficial for facilitating ion transport, increasing the number of active sites, and providing larger space for ion storage. The porosity of biochar-based HPC can be effectively enhanced by applying the hard-templating method [17, 64]. The hard template can attach to biochar, which is then removed with acid or base treatment to stimulate mesopores formation (Fig. 3). The formation of mesopores facilitates the contact between the precursor and activating agent, resulting in increased porosity

297 during activation. For example, an HPC was prepared from porphyra using nickel
298 nanoparticles as the template for mesopore formation [65]. Chen et al. successfully
299 synthesized an EHPC from soybean milk by utilizing simultaneous $CaCO_3$ nanospheres
300 hard template and KOH activation strategy [66]. It should be noted that some biomass
301 contains natural templates such as SiO_2 in rice husk; $CaCO_3$ in soft pitch, and metal-
302 organic framework complexes in *Enteromorpha prolifera*, which could act as self-
303 templates to produce EHPCs during the activation process [27, 67, 68]. The preparation
304 of biochar-based EHPC using these natural templates is known as the self-templating
305 method. The preparation procedure can be performed by major steps, such as pyrolysis,
306 leaching and physical or/and chemical activation [17, 64, 68]; pyrolysis, leaching and
307 further pyrolysis [27].

308 Furthermore, biochar-based EHPC can be prepared via loading metal oxides,
309 heteroatom doping and improving functional groups on biochar-based HPC to further
310 enhance their chemical and electrochemical properties, as shown in Fig. 4. For instance,
311 the coating of Zn(II) on petroleum pitch-derived HPC was synthesized through the
312 impregnation method for dye adsorption [69]. The results exhibited superior adsorption
313 capacities for the Zn/petroleum pitch-derived EHPC compared to the original HPC.
314 That is because Zn coating improved O-containing functional groups, wettability, and
315 active sites, especially the chemisorption via the ZnO/dye interaction. The coating
316 MnO_2 on rice husk biochar-based EHPC was also performed, aiming to enhance the
317 electrochemical properties for SC [13].

318 Heteroatom doping including N, O, P, and S can enhance the electronic
319 conductivity and electrochemical reactivity, thus improving the capacitive behavior of
320 energy storage devices [70]. The elements doping provided stronger chemical
321 adsorption to polysulfide and enhanced electrochemical performance, such as rate

ability, capacity and cycling stability [71, 72], for Li-S batteries. For instance, Jiang et al. synthesized the N, S dual doped lotus plumule-based EHPC interlayer by the one-step method. Note that both N and S contain lone pairs of electrons and the electronegativity of N and S are higher than C. Therefore, the carbon surface had a negative charge after dual-doping N and S. The negative interlayer repulsed the negative Li polysulfides in the electrolyte to the proximity of the S cathode due to electrostatic repulsion. This phenomenon effectively restrained the shuttle of Li polysulfides and improved the capability of the Li-S batteries [73]. Zhu et al. mixed S-doped soybean hull biochar-based EHPC with S in a weight ratio of 2:3 [18].

Notably, some green strategies have also been reported to prepare biochar-based HPC or EHPC. For instance, Liu et al. used sugar cane bagasse to develop N doped EHPC by a green one-step $CaCl_2$ activation with urea [74]. The orange peel act as the green activation reagent and carbon precursor to synthesize N-doped wood powder-based EHPC with ultrahigh yield by only one carbonization step [75]. Some acid constituents and metal elementals in orange peel contributed to the formation of the 3D porous structure. The N-doping was obtained using N-containing components in orange peel. Fishbone was carbonized to produce N-doped EHPC without chemical activation [76]. Fishbone provided a natural $Ca_{10}(PO4)_6(OH)_2$ template and produced abundant heteroatom with N and O content of 5.80 at.% and 7.99 at.%, respectively.

3. Biochar-based HPC/EHPC for supercapacitors

Global energy demand is continuously increasing due to the increase in population and economic growth, which increases greenhouse gas emissions [77, 78]. The development of renewable energy sources is necessary to decrease energy-related carbon emissions. Recent efforts were made to the development of alternative fuel

vehicles (i.e., electric, solar, and hybrid electric vehicles) to lower CO_2 emissions. One of the biggest challenges of these alternative fuel vehicles is to productize a highly efficient electrochemical-based energy storage device. The essential features of these energy storage devices are known as specific capacitance, energy density, power density. The energy density can be determined by the specific capacitance, which is strongly affected by the SSA of the electrode material. The power density is influenced by the electrode resistance, which depends on the diffusion of ions in the electrode porosity [79]. SCs are also called electrical double-layer capacitors (EDLCs), or ultracapacitors received increasing scientific interest due to their high potential applications in the production of energy storage devices [80]. The major challenge of SCs development is to provide a high electrochemical energy storage performance, i.e., specific energy density, high power density, recharging capacity [81].

For enhancing electrochemical energy storage performance, one of the techniques is to improve the electrode porosity. Therefore, the 3D interconnected pore structure of the HPC provides low resistance paths for ions as well as high specific surface area, which have been reported as advanced energy storage materials [38, 82, 83]. On the other hand, another promising approach is to use the Faradaic reactions of surface functional groups on EHPC-based electrodes that can store more energy than the EDL capacitance on conventional capacitor electrodes and provide high power capability [84]. The applications of biochar-based HPCs and EHPCs for SCs are shown in Table 2. Generally, HPCs demonstrated superior capacitive behaviors, i.e., high specific capacitance, energy density, power density, and excellent cycling stability. The Ragone plot of SCs using different biochar-based HPCs and EHPCs is depicted in Fig. 6. The energy density and power density of SCs assembled from biochar-based HPCs and EHPCs (for example, materials-derived from soybean root [85], peanut shell [86],

kraft lignin [23], and ant powder [87]) were greater than or comparable to those of SCs assembled from other materials such as ZIF-derived graphene-based 2D Zn/Co oxide hybrid [88], NiO derived NiO@Ni-MOF composite [89], heteroatoms-doped HPC derived from chitin [90], ultrafine Ni–P@Ni nanotubes [91], HPC nanosheets derived from polymer/graphene oxide hydrogels [92].

3.1. Role of hierarchical porous structure

The hierarchy of carbon materials on porosity, morphological and structural characters are crucial for all kinds of applications to achieve high performance [93]. The synthesis and applications of natural hierarchically porous materials (e.g., biochar-based HPC) received significant attention due to the rapidly evolving topic. The performance of SCs using biochar-based HPC is closely associated with the interconnected hierarchical porous structure, leading to the increase of effective surface area, rapid ionic transport, and efficient charge storage. The major attraction of biochar-based HPC electrodes is that they can achieve very high SSAs. High SSA can provide more active sites, which generally leads to high energy density [94]. Note that the liquid electrolyte is accessible to supermicropores (1–2 nm) and mainly mesopores (2–50 nm) and macropores serve for this purpose, however, it is not applicable for the narrow micropores [95]. The interconnected network of larger pores in biochar-based HPC would provide more favorable and rapid pathways for ions to penetrate. In other words, interconnected pores (i,e., supermicropores, mesopore and macropores) are capable of delivering high power density due to it can be discharged/charged at higher current density [94].

Gou et al. fabricated soybean root biochar-based HPCs-3, 4, and 4.5 through chemical activation with KOH in different ratios of KOH/char = 3, 4, and 4.5,

397 respectively [85]. The SSA of HPC-4 was determined to be 2143 $m^2 g^{-1}$, higher than
398 that of HPC-3 (1708 $m^2 g^{-1}$) and HPC-4.5 (1937 $m^2 g^{-1}$). The mesopore volume of HPC-
399 4 was 0.13 $cm^3 g^{-1}$, which is also much higher than those of HPC-3 (0.01 $cm^3 g^{-1}$) and
400 HPC-4.5 (0.07 $cm^3 g^{-1}$). The hierarchical structure with the co-occurrence of
401 micropores and mesopores in HPCs is beneficial for SCs because the mesopores can
402 rapidly transfer abundant electrolytes to the micropores, thus the charge can effectively
403 accumulate in the micropores, improving the utilization of the micropores. As a result,
404 HPC-4 showed a maximum energy density of as-assembled symmetric SC of 100.5 Wh
405 kg^{-1} at a power density of 4353 W kg^{-1} in neat EMIM BF_4. Moreover, the energy
406 density maintained a high value of 40.7 Wh kg^{-1} at a very high-power density (63000
407 W kg^{-1}).

408 Lately, Peng et al. developed a mixed crab shell and rice husk biochar-based
409 EHPC electrode by a novel strategy through a self-templating method to assemble an
410 SC, as revealed in Fig. 7a [96]. To highlight the benefit of the hierarchical porous
411 structure of the EHPC, a conventional method (non-templating and KOH activation
412 method) was used to prepare single rice husk and crab shell biomass-derived active
413 carbons that are denoted as RH-AC and CS-AC, respectively. The resultant EHPC
414 exhibited a high SSA of 3557 $m^2 g^{-1}$, which was much higher than that of RH-AC (3032
415 $m^2 g^{-1}$) and CS-AC (2109 $m^2 g^{-1}$). The result showed pore contents (macropore,
416 mesopore, and micropore) in EHPC (1.5, 48.5 and 50.0 %), RH-AC (0.0, 14.5, and 85.5
417 %) and CS-AC (1.7, 40 and 58.3 %, respectively). In a two-electrode system with 1 M
418 Na_2SO_4 electrolyte solution, the EHPC-assembled SC showed a high energy density of
419 30.5 W h kg^{-1} at a power density of 225 W kg^{-1}, significantly higher than RH-AC (27.8
420 W h kg−1) and CS-AC (21.6 W h kg^{-1}). The higher electrochemical performance of
421 EHPC was due to its well-developed hierarchical porosity and large SSA.

3.2. Role of functional groups

Additionally, the O-containing functional groups on the biochar-based EHPC surface may be used to enhance the electrochemical performance of SCs [97]. Oxygen functionalities (e.g., phenolic -OH, hydroxyl -OH, quinone -C=O, carboxyl -COOH, and ethers -C-O-C-) can enhance the wettability of the carbon surface and provide additional charge-storage sites. Moreover, Faradaic pseudocapacitance of biochar-based EHPC may be induced by electrochemical reactions at the surface of the electrode in aqueous electrolytes as follows [98]:

$$-C-OH \leftrightarrow -C=O + H^+ + e^- \quad (9)$$

$$-COOH \leftrightarrow -COO + H^+ + e^- \quad (10)$$

$$-C=O + e^- \leftrightarrow -C-O^- \quad (11)$$

The capacitive performance produced by quinone and hydroxyl groups was more effective than that contributed by carboxyl groups in acidic aqueous electrolytes [97]. Liu et al. reported that the O-containing groups (O content of 9.74 at%) of rice husk-based EHPC lead to pseudo-Faradaic reactions and facilitated access of electrolyte species for the construction of the double layer. This could be beneficial for the high-performance SCs with high rate capability and power density [67]. Later, Huang et al. reported the O heteroatom doping in the carbon framework to enhance the wettability of an *Indicalamus* leaves-based EHPC in the aqueous electrolytes. It also delivered a pseudocapacitive contribution to the promoted total capacitance [99]. Zhao et al. reported the production of an O-rich EHPC with abundant functional groups from the carbonization of Artemia cyst shells by HNO_3 treatment and KOH activation. This

study investigated the development of the porosity and surface functional groups and the effect on the electrochemical properties [100]. Most interestingly, the HNO_3 treatment can introduce higher O content to the carbon framework. Even with the EHPC after HNO_3 treatment mostly result in micropores. The suitable wettability benefited from the O rich content and the fast ion transport attributed to the interconnected hierarchical porous structure. Subsequently, it promoted the desolated ions to enter the EHPC micropores more easily. However, O contents slightly decreased after KOH activation. Guo et al. prepared soybean roots-based HPC with the different mass ratios of KOH [85]. Their results showed that the increase of the KOH:biochar ratio from 3, 4, and 4.5 correspond to the decrease of the O contents in EHPCs by 11.5, 8.4, and 8.3 at%, respectively.

In addition, N-doped biochar-based EHPC can improve the pseudocapacitance for SCs, by introducing N in carbon frameworks using N-enriched biomass [76], or employing N-containing precursor [74, 101] or post-treating with ammonia gas. Below reversible redox reactions were proposed for the pseudocapacitance of the N species in the basic electrolyte [102].

$$-CH-NH_2 + 2OH^- \leftrightarrow -C=NH + 2H_2O + 2e^- \quad (12)$$

$$-CH-NH_2 + 2OH^- \leftrightarrow -C-NHOH + H_2O + 2e^- \quad (13)$$

By one-step production, an N-O-S co-doped ant powder-based EHPCs are fabricated for high-performance SCs [87]. Liu et al. investigated the electrochemical energy storage capability of N-O-S co-doped EHPC derived from Kraft lignin [23]. Wan et al. developed an N-O-S co-doped rape pollen-based EHPC [102]. The results indicated that the incorporation of the higher content of heteroatoms (N, O, and S)

effectively improved the hydrophilia of the EHPC and provided additional pseudocapacitance via a redox reaction. More specifically, the higher graphitic N content might produce a higher degree of graphitization, while pyrrolic N could participate in reversible Faradaic reactions and contribute additional pseudocapacitance based on the electron-donor property. The S species in the biochar-based EHPC can act as an electron donor to enhance the surface wettability to facilitate the infiltration of electrolytes, and improve the electrochemical conductivity. Moreover, these S functionalities can contribute to a larger amount of electrochemically active sites, which is important for the reversible pseudocapacitive reactions of sulfones to sulfoxides and sulfoxides to hydroxylated sulfoxides, resulting in enhanced electrochemical energy storage performance.

3.3. Role of electroactive particles

The enhancement of specific capacitance by quick Faradaic reactions can be realized by modifying with electroactive particles of transition metals oxides, such as RuO_2, TiO_2, Cr_2O_3, MnO_2, and Co_2O_3 [98]. Yuan et al. successfully modified MnO_2 on rice husk biochar-based EHPC to enhance the electrochemical properties for SCs [13]. Regardless, the MnO_2-modified EHPC electrode exhibited a higher current response than a pristine HPC and superior charge-storage capacity. At the scan rate of 5 mV s^{-1}, the specific capacitance of the MnO_2-modified EHPC electrode reached 197.6 F g^{-1} in 0.5 M Na_2SO_4 solution, which is approximately 1.5 times higher than that of non-modified HPC under similar conditions. This enhancement is due to the introduction of pseudocapacitive reactions. However, the pristine HPC exhibits excellent capacitance retention with up to 98.5% after 5000 charge-discharge cycles, while that of MnO_2/HPC composite showed only 80.2%. The decay in the capacitance retention may be due to:

(1) disruption of hierarchically porous structure, (2) electrochemical dissolution of MnO_2 into electrolyte, or (3) desquamation of MnO_2 from HPC framework.

Recently, Yuan et al. reported the fabrication of a chicken bone-based EHPC scaffold-MnO_2 (EHPC@MnO_2) nanohybrids for asymmetric SC (Fig. 7b) [24]. EHPC@MnO_2 nanohybrids presented a high specific capacitance of 476.4 F g^{-1} at 1 A g^{-1}. The asymmetric SC exhibited an excellent capacitance and rate performance, delivering a specific energy density of up to 60.8 Wh kg^{-1} at a power density of 1400 W kg^{-1} in 1 M Na_2SO_4 electrolyte. A crab-based EHPC/$CoFe_2O_4$ composite was fabricated to enhance capacitive performances [25]. The composite material delivered 701.8 F g^{-1} at 1 A g^{-1}, which is significantly higher than a pristine HPC of 320.4 F g^{-1}. Moreover, it displayed an excellent cycling performance over 10000 cycles with 90.9% of capacitance retention. A high energy density of 18.2 Wh kg^{-1} was delivered at a power density of 4992 W kg^{-1} in 1 A g^{-1} in 6 M KOH electrolyte.

4. Biochar-based HPC/EHPC for capacitive deionization

Capacitive deionization (CDI) is a process that deionizes water using an electrical potential difference between a pair of electrodes generally made of porous carbons. It is a promising electrochemical technology for water and wastewater treatments (e.g., desalination, electrosorption of heavy metals and contaminated charge species) [103-106]. Significantly, CDI has many advantages in operation, including low energy consumption for low-salinity desalination (< 4000 ppm), high water recovery, direct energy recovery, no chemical additives, low fouling potential, and environmental friendliness [107, 108]. The working mechanism of CDI is based on the introduced electrical double layer (EDL) models, in which unwanted ions are eliminated from the water via electrosorption on the electrodes [103, 109]. First, a pair of porous electrodes

was applied to an external voltage for the electrosorption of ions. The high concentration of ions was adsorbed at the electrode/solution interface via an EDL formation. Second, once the electrodes are saturated with ions, the voltage is removed to regenerate the electrodes (the desorption period), and the electrical energy can be directly recovered during the discharging step.

The HPC-based electrodes with 3D porous architecture are expected to facilitate ion transportation by reducing the resistance in the pore channel [110]. Moreover, eco-friendly HPC derived from biomass/biochar demonstrates abundant surface functional groups. These characteristics of biochar-based HPC/ EHPC are beneficial for efficient electrosorption [111, 112]. The applications of biochar-based HPC for electrochemical deionization is shown in Table 3. As can be seen, a variety of biomass precursors can be used to prepare biochar-based HPC for desalination. Besides, biochar-based HPC presented a high potential in electrosorption of various pollutants such as heavy metals (Cr and Cu), NH_4^+, and Mg^{2+}. Fig. 8 compares the salt adsorption capacities of biochar-based HPC and EHPC electrodes to those of commercial precursor-based electrodes. Specifically, biochar-based HPC or EHPC electrodes exhibit significantly higher salt adsorption capacities than commercial activated carbon electrodes. They also present higher or comparable capacities than commercial precursor-derived HPC and graphene electrodes.

4.1. CDI performance of HPC/EHPC electrode materials

The electrosorption performance of CDI is primarily governed by the EDL formation at the solution/electrode interface of charged nanopores [109]. It may be affected by the porosity characteristics of the electrode (e.g., SSA, PV, and mesoporosity). Significantly higher electrosorption capacity and rate of biochar-based

HPC electrode were reported compared to commercial activated carbon without hierarchical porous structure. Liu et al. reported the electrosorption rate of CDI for the HPC electrode derived from natural basswood was approximately six times higher than the carbon black electrode [50]. In the hierarchical porous structure of biochar-based HPC, mesopores are favorable for improving the electrosorption capacity by providing superior transport pathways for the solvated ions and more active sites for ions [113]. Meanwhile, Sun et al. mentioned that mesopores inside kelp-based HPC improved not only the ionic conductivity but also the wettability of the material, which is crucial in electrochemical desalination [114].

Cuong et al. compared the electrosorption capacity and rate of the rice husk-derived biochar-based EHPCs (Fig. 9a-c), which were prepared by a natural SiO_2 template [115]. Most notably, the EHPC electrode with higher SSA and mesoporosity provides high electrosorption performance. The electrochemical performance of the EHPC electrode was significantly superior to that of the electrode derived from a commercial activated carbon. Besides, EHPC showed high regeneration ability in 10 regeneration cycles for water softening and removal of Mg^{2+}, NH_4^+, and Cu^{2+}. A lignocellulosic loofa sponge biochar-based HPC was prepared by Feng et al. for improving the electrochemical desalination performance of membrane capacitive deionization (MCDI) [116]. Its hierarchical porous structure provided a remarkable specific capacitance of 93.0 F g^{-1} at 5 mV s^{-1} in 1 M NaCl solution and acquired a superior electrosorption capacity of 22.5 mg g^{-1}.

The electrosorption performance was enhanced by introducing pseudocapacitive reactions. Along with a Faradaic charge transfer occurring on the surface or near-surface of the electrode materials. Functional groups on the electrode surface (e.g., oxygen and nitrogen) can enhance the Faradaic capacitance [117, 118].

572 Besides, pseudocapacitive materials (e.g., MnO_2) which have a high theoretical
573 capacitance enhance the electrochemical properties of the material [119]. It should be
574 noted that the N doping on the EHPC surface enhances the electrochemical properties
575 [120, 121]. N functional groups could provide uneven surface charge distributions and
576 generate surface polar active sites. The unsaturated sites of N on the EHPC surface can
577 improve the wettability. Especially pseudocapacitance for Na^+ storage. The pyridinic
578 N and pyrrolic N can increase the electrical conductivity and electroactivity. Meanwhile,
579 the graphitic-N and pyridine-N-oxide are positively charged and promoted electron
580 transfer within the carbon matrix [122].
581
582 The surface O functional groups (e.g., C=O and OH) on HPC are strongly
583 related to the CDI performance because the O functional groups at the carbon surface
584 can enhance the Faradaic capacitance [117]. Electrode materials with moderate O
585 functional groups can contribute to a superior electrosorption capacity, rate, and charge
586 efficiency due to slight chemical oxidation. Liu et al. reported the improvement of CDI
587 performance using a natural basswood biochar-based HPC electrode. The presence of
588 O functional groups on the surface improves the hydrophilicity and wettability [50].
589 The hydrophilicity/wettability of the electrode surfaces was also beneficial for the
590 performance of CDI [123, 124]. However, the O functional groups of electrode
591 materials had a negligible influence on the long-term stability of CDI [125]. The
592 presence of higher O functional groups may affect the electrosorption capacity and
593 charge efficiency [126].
594 Adorna et al. developed coconut shell biochar-based HPC and MnO_2
595 nanocomposite for CDI applications [119]. The MnO_2/HPC electrode can act as the
596 Faradaic/EDL hybrid capacitor to enhance the CDI performance. It showed an excellent

electrosorption capacity of 68.4 mg g^{-1} at an initial NaCl concentration of 1000 mg L^{-1} and 1.2 V. Besides, the performance of HPC-based CDI improved through the increase of the electrical conductivity of the electrode. Typically, graphene is a high conductivity material, which can efficiently promote the electrochemical behavior of carbon electrodes [127, 128]. Feng and his group developed an auricularia biochar-based EHPC electrode coupled with graphene nanosheets. The result showed remarkable improvement in the NaCl electrosorption capacity from 3.90 to 7.74 mg g^{-1} [113].

4.2. Influence of operation conditions on CDI performance

Operation conditions such as the applied voltage and electrolyte concentration play a crucial role in the EDL formation as well as the CDI performance. The applied voltage is an important parameter affecting CDI performance. Zhao et al. observed that the salt adsorption capacity of CDI for used watermelon peel-based HPC increased from 5.84 to 13.56 mg g^{-1} when the voltage increased from 0.8 to 1.4 V [111]. Indicating that the electrostatic forces become stronger, resulting in the formation of the thicker EDL and favoring electro-adsorption of CDI. Additionally, an increased CDI performance was observed from an eggplant-based HPC electrode at a higher initial concentration of NaCl [112]. The electrosorption capacity of this electrode was 14.2 and 33.1 mg L^{-1} with the initial concentration of NaCl of 40 and 1000 mg L^{-1}, respectively. It can be explained by the fact that the compression in the EDL thickness and higher concentration gradation for ion transport. On the other hand, the faster electrosorption rate might be due to the increased conductivity and rapid transport of ions of the electrolyte [111]. Moreover, the eggplant-based HPC also showed a high potential for electrosorption of heavy metals from an aqueous solution (99.1% for Pb^{2+}

and 97.9% for Cd^{2+}). Also, the CDI system maintained high removal efficiencies for Pb^{2+} and Cd^{2+} after three regeneration cycles.

5. Future perspectives

Although the implementation of low-cost biochar-based HPC exhibited promising results in various applications, such as electrochemical deionization, and electrochemical energy storage, it was seen that some critical challenges need to be addressed. Research efforts continued to optimize the material fabrication, aiming to improve porosity properties, simplify processing steps, reduce component costs, enhance application performance, and especially encourage the environmental friendliness of the materials. Based on this review, future research perspectives relating to the advancement of biochar-based HPC and its applications are proposed as the following:

5.1. Selection of specific biomass for innovative electrochemical applications

The utilization of biomass for the synthesis of HPC or EHPC can provide an efficient, economical, and sustainable solution. The selection of biomass is strongly related to the high performance of target HPC or EHPC. Various biomass precursors such as shrimp shell, silkworm cocoon, *Indicalamus* leaf, *Enteromorpha prolifera*, rice husk, soybean root, and peanut shell should be studied in detail for the synthesis of HPC or EHPC. This is because their natural properties can play a crucial role in the pore development of biochar-based HPC with very high SSA (over 2000 m^2 g^{-1}). Using additive templates in the preparation of biochar-based EHPC is beneficial for pore development. However, the use of commercial templates has limitations related to production costs. Some biomass contains templates such as SiO_2 in rice husk, and

organic complexes template in *Indicalamus* leaf should be particularly utilized for HPC fabrication. The design of micropore- or mesopore-dominant biochar-based HPC can be performed through the selection of biomass precursors. Soybean root, corn husk, bagasse-based HPC exhibited as micropore-dominant materials, while oyster shell, *Enteromorpha prolifera*, silk, peanut shell, and rice husk-based HPC are mesopore-dominant materials. In addition to focusing on developing 3D structures in biochar-based HPC to improve electrochemical performance, the development of functional groups on the surface should also have more investigations. Biomass containing N such as algae, peanut shell, and fishbone should be used as potential precursors to prepare N-doped EHPC. On the other hand, N and S-containing precursors such as kraft lignin, barley, and shaddock endothelium can be used to develop N-S co-doped biochar-based EHPC.

5.2. Sustainable process to produce biochar-based HPC

Currently, practicing chemical activation methods based on chemical agents such as KOH, H_3PO_4, and $ZnCl_2$ is most popular and proven effective for the development of porosity with ultrahigh SSA of over 3000 $m^2\ g^{-1}$. However, these chemical agents can cause unfriendly environmental effects. It can be expected that there is an opportunity to replace them with more efficient and less expensive alternatives. For the solution to improve the pore development in the chemical activation process, it should be considered in conjunction with CO_2 as an environmentally friendly agent, especially for producing mesopore-dominant biochar-based HPC.

Controlling the porous structure of biochar-based HPC (mainly mesoporosity and pore size distribution) during the pore development processes (template removal or

activation) is desirable to attain a fast transport and high storage capacity of ions or molecules. Related to the selection of biomass/biochar, the preparation of biochar-based HPC or EHPC by a green templating method requires more attention. The use of natural template presents in biomass precursor (e.g., SiO_2 in rice husk) or natural material as an additive template (e.g., $CaCO_3$ in the oyster shell) should be preferred. Besides, a green activation strategy can also be used to develop the biochar-based HPC or EHPC. In the green activation, it is suggested that adding natural (e.g., orange peel), or green (e.g., $CaCl_2$) activation agent can help to make the green process. In addition, a non-activation process is also a sustainable approach to develop HPC or EHPC. However, this approach depends on the discovery and selection of special biomass such as herringbone, *Indicalamus* leaves with their unique chemical composition and structure. Furthermore, the utilization of the green activation strategy can enhance the yield. In general, the synthesis of biochar-based HPC should be performed on a large-scale with controlling parameters to optimize yield.

5.3. Challenges and prospects for advanced HPC/EHPC

Challenges remain in the use of biochar-based HPC or EHPC in electrochemical deionization, including achievements of efficient desalination efficiency, superior electrosorption capacity, and high-water recovery. It is obligatory to further improve the ion-accessible SSA, ion mobility within the pore network, electrochemical stability over the pH, voltage range, and electronic conductivity. It is necessary to have a comprehensive assessment of the effect of heteroatom doping (e.g., N, O, S, and P) on electrochemical deionization performance. The design of biochar-based EHPC using metal oxides, e.g., MnO_2, TiO_2, and Co_3O_4 may enhance wettability, electrocatalysis, specific capacitance, and improved charge separation. More interestingly, these metal

oxides can provide abundant reaction or interaction sites for surface or interface-related processes such as redox reaction and adsorption. Future perspective is expected to successfully scale up CDI methods using biochar-based HPC or EHPC electrode, particularly for practical applications such as desalination of seawater, electrosorption of industrial wastewater and high-contaminated groundwater by optimization of electrode materials, and operation parameters.

For the application of biochar-based HPC in electrochemical energy storage, the requirement is to maximize energy density to meet future energy needs. Besides, the enhancement of specific capacitance for biochar-based HPC by quick Faradaic reactions can be realized by modification of electroactive particles of transition metal oxides such as RuO_2, TiO_2, Cr_2O_3, MnO_2, and Co_2O_3. However, the design of these metal oxides on biochar-based HPC causes pore blocking, leading to a decrease in the SSA and PV. Therefore, it is necessary to optimize the number of modified substances, avoiding the influence on the hierarchical structure of HPC as well as achieving the best electrochemical performance. Ideally, a biochar-based EHPC-assembled SC is used to deliver energy for an HPC-based CDI system in the water treatment application, which is a promising perspective.

Furthermore, emerging applications of biochar-based HPC should be extended to the pilot-scale to assess technical, economic, and environmental feasibility under practical conditions. The challenges in upscaling mainly involve the acceptance of companies and production facilities, that are using biochar as a precursor to producing HPC. In addition, national policies (such as tax incentives) can be an effective approach in encouraging the use of biomass to produce HPCs.

6. Conclusion

The abundance of lignocellulosic biomass, lower cost, easy accessibility, recyclable properties, higher carbon content, and environmentally friendly nature ensure that the biomass is ideal candidates for resources of porous carbon materials. Similarly, naturally obtained hierarchical porous structure and hetero-atom facilitate electrolyte penetration and generation of additional active sites, respectively, for higher performance. The knowledge gaps that exist in the synthesis and application of biochar-based HPC and EHPCs are discussed. The bio-char-derived EHPC with adjustable physicochemical properties, superb electrical conductivity, satisfactory SSA, and higher electrochemical stability has been attracting significant attention to be a promising candidate for supercapacitors and other energy storage applications. Hence the biochar-based HPC and EHPC are essential to bridge the gap between conventional electrochemical capacitors and rechargeable batteries to meet the increasing energy demand.

An improved comprehension of sustainable, environmentally friendly, and cost-effective biochar-based HPC and EHPC is presented in this review. The biochar-based HPC consists of the 3D interconnected pore structure of micro-, meso-, and macropores, which is beneficial for the transport of ions and providing abundant active sites for an increase in the ion-accessible SSA. The biochar-based EHPC is synthesized or developed with a controllable 3D pore structure, heteroatom-doping, and metal oxides-impregnated surface. The preparation methods of biochar-based HPC or EHPC have been extensively investigated using the hard-template, self-template, or non-template methods. The development of biochar-based EHPC is described to further enhance the physicochemical or electrochemical properties for capacitive charge storage. The insight into mechanisms of hierarchical porous architecture, surface functional groups and additive electroactive particles are investigated on the electrochemical performance

of SCs. To understand the effect of properties of HPC on CDI, the effect of biomass precursors, the role of the hierarchical porous structure, and the role of functional groups of HPC on the CDI are discussed. The development of green sustainable methods for the fabrication of biochar-based HPC and the challenges in capacitive charge storage are highlighted. Most significantly, it indicated that biochar-based HPC or EHPC is a promising material for emerging applications such as environmental remediation, electrochemical deionization, and energy storage. Consequently, the biomass utilization for the synthesis of HPCs should be highly encouraged in the future so that biomass-derived HPCs will bring more exciting results without hampering the environment.

Acknowledgment

This work was supported by the Ministry of Science and Technology, Taiwan (107-2628-E-002-001-MY3; 109-2223-E-002-002-MY3; 108-2638-E-002-003-MY2 (Shackleton Program award)), the National University of Civil Engineering, Vietnam (10-2021/KHXD-TĐ), the National Research Foundation of Korea (NRF) (NRF-2015R1A2A2A11001432) and NRF Germany-Korea Partnership Program (GEnKO Program) (2018–2020). This work was also supported by Hydrogen Energy Innovation Technology Development Program of the National Research Foundation of Korea (NRF) funded by the Korean government (Ministry of Science and ICT(MSIT)) (NRF-2019M3E6A1064197) and Korea University Grant. BS acknowledges support from the Lancaster Environment Centre Project. This research was also supported by the GNin Technology, Taiwan, ARC-Linkage Project (LP180100429), and the Global Connections Fund (Bridging Grant Scheme) of the Australian Academy of Technology and Engineering (ATSE). This work was partially performed in part at the Queensland

771 node of the Australian National Fabrication Facility, a company established under the
772 National Collaborative Research Infrastructure Strategy to provide nano and
773 microfabrication facilities for Australia's researchers.

774

775 **References**

776 [1] Abioye AM, Ani FN. Recent development in the production of activated carbon
777 electrodes from agricultural waste biomass for supercapacitors: A review.
778 Renewable and Sustainable Energy Reviews. 2015;52:1282-93.
779 [2] Matsagar BM, Hossain SA, Islam T, Alamri HR, Alothman ZA, Yamauchi Y, et al.
780 Direct production of furfural in one-pot fashion from raw biomass using
781 brønsted acidic ionic liquids. Scientific Reports. 2017;7:13508.
782 [3] Dang HTT, Dinh CV, Nguyen KM, Tran NTH, Pham TT, Narbaitz RM. Loofah
783 sponges as bio-carriers in a pilot-scale integrated fixed-film activated sludge
784 system for municipal wastewater treatment. Sustainability. 2020;12:4758.
785 [4] Wang J, Nie P, Ding B, Dong SY, Hao XD, Dou H, et al. Biomass derived carbon
786 for energy storage devices. Journal of Materials Chemistry A. 2017;5:2411-28.
787 [5] Liu W-J, Jiang H, Yu H-Q. Emerging applications of biochar-based materials for
788 energy storage and conversion. Energy & Environmental Science.
789 2019;12:1751-79.
790 [6] Tan X-f, Liu Y-g, Gu Y-l, Xu Y, Zeng G-m, Hu X-j, et al. Biochar-based nano-
791 composites for the decontamination of wastewater: A review. Bioresource
792 Technology. 2016;212:318-33.
793 [7] Cuong DV, Wu P-C, Chen L-I, Hou C-H. Active MnO_2/biochar composite for
794 efficient As(III) removal: Insight into the mechanisms of redox transformation
795 and adsorption. Water Research. 2021;188:116495.

[8] Xu G, Han J, Ding B, Nie P, Pan J, Dou H, et al. Biomass-derived porous carbon materials with sulfur and nitrogen dual-doping for energy storage. Green Chemistry. 2015;17:1668-74.

[9] Farma R, Deraman M, Awitdrus A, Talib IA, Taer E, Basri NH, et al. Preparation of highly porous binderless activated carbon electrodes from fibres of oil palm empty fruit bunches for application in supercapacitors. Bioresource Technology. 2013;132:254-61.

[10] Liao Y-T, Matsagar BM, Wu KCW. Metal–organic framework (MOF)-derived effective solid catalysts for valorization of lignocellulosic biomass. ACS Sustainable Chemistry & Engineering. 2018;6:13628-43.

[11] Glotzer SC. Assembly engineering: Materials design for the 21st century (2013 P.V. Danckwerts lecture). Chemical Engineering Science. 2015;121:3-9.

[12] Gielen D, Boshell F, Saygin D. Climate and energy challenges for materials science. Nature Materials. 2016;15:117.

[13] Yuan CJ, Lin HB, Lu HY, Xing ED, Zhang YS, Xie BY. Synthesis of hierarchically porous MnO_2/rice husks derived carbon composite as high-performance electrode material for supercapacitors. Applied Energy. 2016;178:260-8.

[14] Wang GQ, Wang DL, Kuang S, Xing W, Zhuo SP. Hierarchical porous carbon derived from rice husk as a low-cost counter electrode of dye-sensitized solar cells. Renewable Energy. 2014;63:708-14.

[15] Karatum O, Steiner SA, 3rd, Griffin JS, Shi W, Plata DL. Flexible, mechanically durable aerogel composites for oil capture and recovery. ACS Applied Materials & Interfaces. 2016;8:215-24.

[16] Lin KYA, Chang HA, Chen BJ. Multi-functional MOF-derived magnetic carbon sponge. Journal of Materials Chemistry A. 2016;4:13611-25.

[17] Cuong DV, Liu NL, Nguyen VA, Hou CH. Meso/micropore-controlled hierarchical porous carbon derived from activated biochar as a high-performance adsorbent for copper removal. Science of The Total Environment. 2019;692:844-53.

[18] Zhu Y, Xu GY, Zhang XL, Wang SJ, Li C, Wang GX. Hierarchical porous carbon derived from soybean hulls as a cathode matrix for lithium-sulfur batteries. Journal of Alloys and Compounds. 2017;695:2246-52.

[19] Wan L, Xiao R, Liu J, Zhang Y, Chen J, Du C, et al. A novel strategy to prepare N, S-codoped porous carbons derived from barley with high surface area for supercapacitors. Applied Surface Science. 2020;518:146265.

[20] Hulicova-Jurcakova D, Seredych M, Lu GQ, Bandosz TJ. Combined effect of nitrogen-and oxygen-containing functional groups of microporous activated carbon on its electrochemical performance in supercapacitors. Advanced Functional Materials. 2009;19:438-47.

[21] Van Nguyen C, Boo JR, Liu C-H, Ahamad T, Alshehri SM, Matsagar BM, et al. Oxidation of biomass-derived furans to maleic acid over nitrogen-doped carbon catalysts under acid-free conditions. Catalysis Science & Technology. 2020;10:1498-506.

[22] Chen L, Zhang YZ, Lin CH, Yang W, Meng Y, Guo Y, et al. Hierarchically porous nitrogen-rich carbon derived from wheat straw as an ultra-high-rate anode for lithium ion batteries. Journal of Materials Chemistry A. 2014;2:9684-90.

[23] Liu FY, Wang ZX, Zhang HT, Jin L, Chu X, Gu BN, et al. Nitrogen, oxygen and sulfur co-doped hierarchical porous carbons toward high-performance supercapacitors by direct pyrolysis of kraft lignin. Carbon. 2019;149:105-16.

[24] Yuan X, Zhang Y, Yan Y, Wei B, Qiao K, Zhu B, et al. Tunable synthesis of biomass-based hierarchical porous carbon scaffold@ MnO_2 nanohybrids for asymmetric supercapacitor. Chemical Engineering Journal. 2019.

[25] Fu M, Chen W, Ding JX, Zhu XX, Liu QY. Biomass waste derived multi-hierarchical porous carbon combined with CoFe2O4 as advanced electrode materials for supercapacitors. Journal of Alloys and Compounds. 2019;782:952-60.

[26] Rybarczyk MK, Peng HJ, Tang C, Lieder M, Zhang Q, Titirici MM. Porous carbon derived from rice husks as sustainable bioresources: insights into the role of micro-/mesoporous hierarchy in hosting active species for lithium-sulphur batteries. Green Chemistry. 2016;18:5169-79.

[27] Gao F, Geng C, Xiao N, Qu JY, Qiu JS. Hierarchical porous carbon sheets derived from biomass containing an activation agent and in-built template for lithium ion batteries. Carbon. 2018;139:1085-92.

[28] Sun JT, Niu J, Liu MY, Ji J, Dou ML, Wang F. Biomass-derived nitrogen-doped porous carbons with tailored hierarchical porosity and high specific surface area for high energy and power density supercapacitors. Applied Surface Science. 2018;427:807-13.

[29] Peng L, Liang YR, Huang JY, Xing LL, Hu H, Xiao Y, et al. Mixed-biomass wastes derived hierarchically porous carbons for high-performance electrochemical energy storage. ACS Sustainable Chemistry & Engineering. 2019;7:10393-402.

[30] Zhang YC, You Y, Xin S, Yin YX, Zhang J, Wang P, et al. Rice husk-derived hierarchical silicon/nitrogen-doped carbon/carbon nanotube spheres as low-cost and high-capacity anodes for lithium-ion batteries. Nano Energy. 2016;25:120-7.

[31] Ge X, Ma Y, Song X, Wang G, Zhang H, Zhang Y, et al. β-FeOOH nanorods/carbon foam-based hierarchically porous monolith for highly effective arsenic removal. ACS Applied Materials & Interfaces. 2017;9:13480-90.

[32] Sun JT, Zhang ZP, Ji J, Dou ML, Wang F. Removal of Cr^{6+} from wastewater via adsorption with high-specific-surface-area nitrogen-doped hierarchical porous carbon derived from silkworm cocoon. Applied Surface Science. 2017;405:372-9.

[33] Yu DY, Wang LL, Wu MH. Simultaneous removal of dye and heavy metal by banana peels derived hierarchically porous carbons. Journal of the Taiwan Institute of Chemical Engineers. 2018;93:543-53.

[34] Yin WQ, Dai D, Hou JH, Wang SS, Wu XG, Wang XZ. Hierarchical porous biochar-based functional materials derived from biowaste for Pb(II) removal. Applied Surface Science. 2019;465:297-302.

[35] Chen L, Ji T, Mu L, Shi Y, Wang H, Zhu J. Pore size dependent molecular adsorption of cationic dye in biomass derived hierarchically porous carbon. Journal of Environmental Management. 2017;196:168-77.

[36] Qin L, Zhou ZP, Dai JD, Ma P, Zhao HB, He JS, et al. Novel N-doped hierarchically porous carbons derived from sustainable shrimp shell for high-performance removal of sulfamethazine and chloramphenicol. Journal of the Taiwan Institute of Chemical Engineers. 2016;62:228-38.

[37] Dai JD, Qin L, Zhang RL, Xie AT, Chang ZS, Tian SJ, et al. Sustainable bovine bone-derived hierarchically porous carbons with excellent adsorption of antibiotics: Equilibrium, kinetic and thermodynamic investigation. Powder Technology. 2018;331:162-70.

[38] Huang CH, Zhang Q, Chou TC, Chen CM, Su DS, Doong RA. Three-dimensional hierarchically ordered porous carbons with partially graphitic nanostructures for electrochemical capacitive energy storage. ChemSusChem. 2012;5:563-71.

[39] Matsagar BM, Yang R-X, Dutta S, Ok YS, Wu KCW. Recent progress in the development of biomass-derived nitrogen-doped porous carbon. Journal of Materials Chemistry A. 2021, DOI: 10.1039/d0ta09706c.

[40] Sohi S, Lopez-Capel E, Krull E, Bol R. Biochar, climate change and soil: A review to guide future research. CSIRO Land and Water Science Report. 2009;5:17-31.

[41] Khan JH, Lin J, Young C, Matsagar BM, Wu KCW, Dhepe PL, et al. High surface area nanoporous carbon derived from high quality jute from Bangladesh. Materials Chemistry and Physics. 2018;216:491-5.

[42] Kim KH, Kim T-S, Lee S-M, Choi D, Yeo H, Choi I-G, et al. Comparison of physicochemical features of biooils and biochars produced from various woody biomasses by fast pyrolysis. Renewable Energy. 2013;50:188-95.

[43] Sangjan A, Ngamsiri P, Klomkliang N, Wu KCW, Matsagar BM, Ratchahat S, et al. Effect of microwave-assisted wet torrefaction on liquefaction of biomass from palm oil and sugarcane wastes to bio-oil and carbon nanodots/nanoflakes by hydrothermolysis and solvothermolysis. Renewable Energy. 2020;154:1204-17.

916 [44] Dutta S, Bhaumik A, Wu KCW. Hierarchically porous carbon derived from
917 polymers and biomass: effect of interconnected pores on energy applications.
918 Energy & Environmental Science. 2014;7:3574-92.
919 [45] Zhong RY, Sels BF. Sulfonated mesoporous carbon and silica-carbon
920 nanocomposites for biomass conversion. Applied Catalysis B: Environmental.
921 2018;236:518-45.
922 [46] Tian ZW, Qiu Y, Zhou JC, Zhao XB, Cai JJ. The direct carbonization of algae
923 biomass to hierarchical porous carbons and CO_2 adsorption properties.
924 Materials Letters. 2016;180:162-5.
925 [47] Hao P, Zhao Z, Tian J, Li H, Sang Y, Yu G, et al. Hierarchical porous carbon
926 aerogel derived from bagasse for high performance supercapacitor electrode.
927 Nanoscale. 2014;6:12120-9.
928 [48] Zhang Z, Wang K, Atkinson JD, Yan X, Li X, Rood MJ, et al. Sustainable and
929 hierarchical porous Enteromorpha prolifera based carbon for CO_2 capture.
930 Journal of Hazardous Materials. 2012;229-230:183-91.
931 [49] Dutta S, Huang SY, Chen C, Chen JE, Alothman ZA, Yamauchi Y, et al. Cellulose
932 framework directed construction of hierarchically porous carbons offering high-
933 performance capacitive deionization of brackish water. ACS Sustainable
934 Chemistry & Engineering. 2016;4:1885-93.
935 [50] Liu M, Xu M, Xue Y, Ni W, Huo S, Wu L, et al. Efficient capacitive deionization
936 using natural basswood derived, free standing, hierarchically porous carbon
937 electrodes. ACS Applied Materials & Interfaces. 2018.
938 [51] Rodriguez-Reinoso F, Molina-Sabio M. Activated carbons from lignocellulosic
939 materials by chemical and/or physical activation: An overview. Carbon.
940 1992;30:1111-8.

941 [52] Bazan-Wozniak A, Nowicki P, Pietrzak R. Removal of NO_2 from gas stream by
942 activated bio-carbons from physical activation of residue of supercritical
943 extraction of hops. Chemical Engineering Research and Design. 2021;166:67-
944 73.
945 [53] Bardestani R, Kaliaguine S. Steam activation and mild air oxidation of vacuum
946 pyrolysis biochar. Biomass and Bioenergy. 2018;108:101-12.
947 [54] Zhang TY, Walawender WP, Fan LT, Fan M, Daugaard D, Brown RC. Preparation
948 of activated carbon from forest and agricultural residues through CO_2 activation.
949 Chemical Engineering Journal. 2004;105:53-9.
950 [55] Xin-Hui D, Srinivasakannan C, Jin-Hui P, Li-Bo Z, Zheng-Yong Z. Comparison
951 of activated carbon prepared from Jatropha hull by conventional heating and
952 microwave heating. Biomass and Bioenergy. 2011;35:3920-6.
953 [56] Cheng F, Li XW. Preparation and application of biochar-based catalysts for biofuel
954 production. Catalysts. 2018;8:346.
955 [57] Ramanayaka S, Tsang DCW, Hou D, Ok YS, Vithanage M. Green synthesis of
956 graphitic nanobiochar for the removal of emerging contaminants in aqueous
957 media. Science of The Total Environment. 2020;706:135725.
958 [58] Rajapaksha AU, Chen SS, Tsang DCW, Zhang M, Vithanage M, Mandal S, et al.
959 Engineered/designer biochar for contaminant removal/immobilization from soil
960 and water: Potential and implication of biochar modification. Chemosphere.
961 2016;148:276-91.
962 [59] Dissanayake PD, Choi SW, Igalavithana AD, Yang X, Tsang DCW, Wang C-H,
963 et al. Sustainable gasification biochar as a high efficiency adsorbent for CO_2
964 capture: A facile method to designer biochar fabrication. Renewable and
965 Sustainable Energy Reviews. 2020;124:109785.

966 [60] Wei X, Zhang ZD, Qin L, Dai JD. Template-free preparation of yeast-derived
967 three-dimensional hierarchical porous carbon for highly efficient
968 sulfamethazine adsorption from water. Journal of the Taiwan Institute of
969 Chemical Engineers. 2019;95:532-40.
970 [61] Ao WY, Fu J, Mao X, Kang QH, Ran CM, Liu Y, et al. Microwave assisted
971 preparation of activated carbon from biomass: A review. Renew Sust Energ Rev.
972 2018;92:958-79.
973 [62] Li W, Liu J, Zhao D. Mesoporous materials for energy conversion and storage
974 devices. Nature Reviews Materials. 2016;1:1-17.
975 [63] Prabaharan SRS, Vimala R, Zainal Z. Nanostructured mesoporous carbon as
976 electrodes for supercapacitors. Journal of Power Sources. 2006;161:730-6.
977 [64] Kim J, Yi Y, Peck DH, Yoon SH, Jung DH, Park HS. Controlling hierarchical
978 porous structures of rice-husk-derived carbons for improved capacitive
979 deionization performance. Environmental Science: Nano. 2019;6:916-24.
980 [65] Ouyang HB, Gong QQ, Li CY, Huang JF, Xu ZW. Porphyra derived hierarchical
981 porous carbon with high graphitization for ultra-stable lithium-ion batteries.
982 Materials Letters. 2019;235:111-5.
983 [66] Chen MF, Yu D, Zheng XZ, Dong XP. Biomass based N-doped hierarchical
984 porous carbon nanosheets for all-solid-state supercapacitors. Journal of Energy
985 Storage. 2019;21:105-12.
986 [67] Liu DC, Zhang WL, Lin HB, Li Y, Lu HY, Wang Y. Hierarchical porous carbon
987 based on the self-templating structure of rice husk for high-performance
988 supercapacitors. RSC Advances. 2015;5:19294-300.
989 [68] Gao Y, Zhang WL, Yue QY, Gao BY, Sun YY, Kong JJ, et al. Simple synthesis
990 of hierarchical porous carbon from Enteromorpha prolifera by a self-template

method for supercapacitor electrodes. Journal of Power Sources. 2014;270:403-10.

[69] Zhang C, Li Y, Li Y, Zhang W, Wang X, He X, et al. Synthesis and Zn(II) modification of hierarchical porous carbon materials from petroleum pitch for effective adsorption of organic dyes. Chemosphere. 2019;216:379-86.

[70] Cai JJ, Wu C, Zhu Y, Zhang KL, Shen PK. Sulfur impregnated N, P co-doped hierarchical porous carbon as cathode for high performance Li-S batteries. Journal of Power Sources. 2017;341:165-74.

[71] Rehman S, Guo S, Hou Y. Rational design of Si/SiO_2 @hierarchical porous carbon spheres as efficient polysulfide reservoirs for high-performance Li-S battery. Advanced Materials. 2016;28:3167-72.

[72] Zhang XQ, Cui YL, Zhong Y, Wang DH, Tang WJ, Wang XL, et al. Cobalt disulfide-modified cellular hierarchical porous carbon derived from bovine bone for application in high-performance lithium–sulfur batteries. Journal of Colloid and Interface Science. 2019;551:219-26.

[73] Jiang SX, Chen MF, Wang XY, Zhang Y, Huang C, Zhang YP, et al. Honeycomb-like nitrogen and sulfur dual-doped hierarchical porous biomass carbon bifunctional interlayer for advanced lithium-sulfur batteries. Chemical Engineering Journal. 2019;355:478-86.

[74] Liu J, Deng Y, Li X, Wang L. Promising nitrogen-rich porous carbons derived from one-step calcium chloride activation of biomass-based waste for high performance supercapacitors. ACS Sustainable Chemistry & Engineering. 2016;4:177-87.

[75] Wang C, Wang H, Dang B, Wang Z, Shen X, Li C, et al. Ultrahigh yield of nitrogen doped porous carbon from biomass waste for supercapacitor. Renewable Energy. 2020;156:370-6.

[76] Mu J, Wong SI, Li Q, Zhou P, Zhou J, Zhao Y, et al. Fishbone-derived N-doped hierarchical porous carbon as an electrode material for supercapacitor. Journal of Alloys and Compounds. 2020;832:154950.

[77] van Ruijven BJ, De Cian E, Wing IS. Amplification of future energy demand growth due to climate change. Nature Communications. 2019;10:2762.

[78] Jones GA, Warner KJ. The 21st century population-energy-climate nexus. Energy Policy. 2016;93:206-12.

[79] Conway BE. Electrochemical supercapacitors: scientific fundamentals and technological applications: Springer Science & Business Media; 2013.

[80] Nakajima T, Groult H. Advanced fluoride-based materials for energy conversion: Elsevier; 2015.

[81] Bi Z, Kong Q, Cao Y, Sun G, Su F, Wei X, et al. Biomass-derived porous carbon materials with different dimensions for supercapacitor electrodes: a review. Journal of Materials Chemistry A. 2019;7:16028-45.

[82] Xia W, Qiu B, Xia DG, Zou RQ. Facile preparation of hierarchically porous carbons from metal-organic gels and their application in energy storage. Scientific Reports. 2013;3:1935.

[83] Sun H, Zhu J, Baumann D, Peng L, Xu Y, Shakir I, et al. Hierarchical 3D electrodes for electrochemical energy storage. Nature Reviews Materials. 2019;4:45-60.

[84] Lee SW, Yabuuchi N, Gallant BM, Chen S, Kim BS, Hammond PT, et al. High-power lithium batteries from functionalized carbon-nanotube electrodes. Nature Nanotechnology. 2010;5:531-7.

[85] Guo NN, Li M, Wang Y, Sun XK, Wang F, Yang R. Soybean root-derived hierarchical porous carbon as electrode material for high-performance supercapacitors in ionic liquids. ACS Applied Materials & Interfaces. 2016;8:33626-34.

[86] Ding J, Wang HL, Li Z, Cui K, Karpuzov D, Tan XH, et al. Peanut shell hybrid sodium ion capacitor with extreme energy-power rivals lithium ion capacitors. Energy & Environmental Science. 2015;8:941-55.

[87] Zhao G, Chen C, Yu D, Sun L, Yang C, Zhang H, et al. One-step production of ONS co-doped three-dimensional hierarchical porous carbons for high-performance supercapacitors. Nano Energy. 2018;47:547-55.

[88] Yu J, Cui Z, Li X, Chen D, Ji J, Zhang Q, et al. Facile fabrication of ZIF-derived graphene-based 2D Zn/Co oxide hybrid for high-performance supercapacitors. Journal of Energy Storage. 2020;27:101165.

[89] Xiong S, Jiang S, Wang J, Lin H, Lin M, Weng S, et al. A high-performance hybrid supercapacitor with NiO derived NiO@Ni-MOF composite electrodes. Electrochimica Acta. 2020;340:135956.

[90] Wang Y, Liu R, Tian Y, Sun Z, Huang Z, Wu X, et al. Heteroatoms-doped hierarchical porous carbon derived from chitin for flexible all-solid-state symmetric supercapacitors. Chemical Engineering Journal. 2020;384:123263.

[91] Li W, Wu M, Shi P, Li T, Yue H, Dong Z, et al. Enhanced energy storage performance of advanced hybrid supercapacitors derived from ultrafine Ni–P@Ni nanotubes with novel three-dimensional porous network synthesized via reaction temperatures regulation. Electrochimica Acta. 2020;331:135440.

[92] Wang M, Yang J, Liu S, Li M, Hu C, Qiu J. Nitrogen-doped hierarchically porous carbon nanosheets derived from polymer/graphene oxide hydrogels for high-

performance supercapacitors. Journal of Colloid and Interface Science. 2020;560:69-76.

[93] Yang X-Y, Chen L-H, Li Y, Rooke JC, Sanchez C, Su B-L. Hierarchically porous materials: synthesis strategies and structure design. Chemical Society Reviews. 2017;46:481-558.

[94] Xing W, Qiao SZ, Ding RG, Li F, Lu GQ, Yan ZF, et al. Superior electric double layer capacitors using ordered mesoporous carbons. Carbon. 2006;44:216-24.

[95] Fuertes AB, Pico F, Rojo JM. Influence of pore structure on electric double-layer capacitance of template mesoporous carbons. Journal of Power Sources. 2004;133:329-36.

[96] Peng L, Liang Y, Huang J, Xing L, Hu H, Xiao Y, et al. Mixed-biomass wastes derived hierarchically porous carbons for high-performance electrochemical energy storage. ACS Sustainable Chemistry & Engineering. 2019.

[97] He YT, Zhang YH, Li XF, Lv Z, Wang XJ, Liu ZG, et al. Capacitive mechanism of oxygen functional groups on carbon surface in supercapacitors. Electrochimica Acta. 2018;282:618-25.

[98] Frackowiak E, Beguin F. Carbon materials for the electrochemical storage of energy in capacitors. Carbon. 2001;39:937-50.

[99] Huang J, Chen L, Dong H, Zeng Y, Hu H, Zheng M, et al. Hierarchical porous carbon with network morphology derived from natural leaf for superior aqueous symmetrical supercapacitors. Electrochimica Acta. 2017;258:504-11.

[100] Zhao Y, Ran W, He J, Song Y, Zhang C, Xiong DB, et al. Oxygen-rich hierarchical porous carbon derived from artemia cyst shells with superior electrochemical performance. ACS Applied Materials & Interfaces. 2015;7:1132-9.

[101] Jiang X, Guo F, Jia X, Zhan Y, Zhou H, Qian L. Synthesis of nitrogen-doped hierarchical porous carbons from peanut shell as a promising electrode material for high-performance supercapacitors. Journal of Energy Storage. 2020;30:101451.

[102] Wan L, Wei W, Xie MJ, Zhang Y, Li X, Xiao R, et al. Nitrogen, sulfur co-doped hierarchically porous carbon from rape pollen as high-performance supercapacitor electrode. Electrochimica Acta. 2019;311:72-82.

[103] Choi J, Dorji P, Shon HK, Hong S. Applications of capacitive deionization: Desalination, softening, selective removal, and energy efficiency. Desalination. 2019;449:118-30.

[104] Chen ZL, Zhang HT, Wu CX, Wang YS, Li W. A study of electrosorption selectivity of anions by activated carbon electrodes in capacitive deionization. Desalination. 2015;369:46-50.

[105] Hemmatifar A, Ramachandran A, Liu K, Oyarzun DI, Bazant MZ, Santiago JG. Thermodynamics of ion separation by electrosorption. Environmental Science & Technology. 2018;52:10196-204.

[106] Zornitta RL, Ruotolo LA. Simultaneous analysis of electrosorption capacity and kinetics for CDI desalination using different electrode configurations. Chemical Engineering Journal. 2018;332:33-41.

[107] Chen YW, Chen JF, Lin CH, Hou CH. Integrating a supercapacitor with capacitive deionization for direct energy recovery from the desalination of brackish water. Applied Energy. 2019;252:113417.

[108] Shiu H-Y, Lee M, Chao Y, Chang K-C, Hou C-H, Chiueh P-T. Hotspot analysis and improvement schemes for capacitive deionization (CDI) using life cycle assessment. Desalination. 2019;468:114087.

[109] AlMarzooqi FA, Al Ghaferi AA, Saadat I, Hilal N. Application of capacitive deionisation in water desalination: A review. Desalination. 2014;342:3-15.

[110] Baroud TN, Giannelis EP. Role of mesopore structure of hierarchical porous carbons on the electrosorption performance of capacitive deionization electrodes. ACS Sustainable Chemistry & Engineering. 2019;7:7580-96.

[111] Zhao SS, Yan TT, Wang Z, Zhang JP, Shi LY, Zhang DS. Removal of NaCl from saltwater solutions using micro/mesoporous carbon sheets derived from watermelon peel via deionization capacitors. RSC Advances. 2017;7:4297-305.

[112] Zhao CJ, Zhang SB, Sun N, Zhou HJ, Wang GZ, Zhang YX, et al. Converting eggplant biomass into multifunctional porous carbon electrodes for self-powered capacitive deionization. Environmental Science: Water Research & Technology. 2019;5:1054-63.

[113] Feng J, Yang ZY, Hou SY, Li MZ, Lv RT, Kang FY, et al. GO/auricularia-derived hierarchical porous carbon used for capacitive deionization with high performance. Colloids and Surfaces A: Physicochemical and Engineering Aspects. 2018;547:134-40.

[114] Sun N, Li ZY, Zhang X, Qin WX, Zhao CJ, Zhang HM, et al. Hierarchical porous carbon materials derived from kelp for superior capacitive applications. ACS Sustainable Chemistry & Engineering. 2019;7:8735-43.

[115] Cuong DV, Wu P-C, Liu N-L, Hou C-H. Hierarchical porous carbon derived from activated biochar as an eco-friendly electrode for the electrosorption of inorganic ions. Separation and Purification Technology. 2020;242:116813.

[116] Feng CJ, Chen YA, Yu CP, Hou CH. Highly porous activated carbon with multi-channeled structure derived from loofa sponge as a capacitive electrode material for the deionization of brackish water. Chemosphere. 2018;208:285-93.

[117] Su H, Lian C, Gallegos A, Deng S, Shang Y, Liu H, et al. Microscopic insights into the Faradaic reaction effects on the electric double layers. Chemical Engineering Science. 2020;215:115452.

[118] Tian S, Wu J, Zhang X, Ostrikov KK, Zhang Z. Capacitive deionization with nitrogen-doped highly ordered mesoporous carbon electrodes. Chemical Engineering Journal. 2020;380:122514.

[119] Adorna Jr J, Borines M, Doong R-A. Coconut shell derived activated biochar–manganese dioxide nanocomposites for high performance capacitive deionization. Desalination. 2020;492:114602.

[120] Zhang R, Gu X, Liu Y, Hua D, Shao M, Gu Z, et al. Hydrophilic nano-porous carbon derived from egg whites for highly efficient capacitive deionization. Applied Surface Science. 2020;512:145740.

[121] Muthukumaraswamy Rangaraj V, Achazhiyath Edathil A, Y. Kannangara Y, Song J-K, Abu Haija M, Banat F. Tamarind shell derived N-doped carbon for capacitive deionization (CDI) studies. Journal of Electroanalytical Chemistry. 2019;848:113307.

[122] Tian S, Wu J, Zhang X, Ostrikov K, Zhang Z. Capacitive deionization with nitrogen-doped highly ordered mesoporous carbon electrodes. Chemical Engineering Journal. 2020;380:122514.

[123] Aslan M, Zeiger M, Jackel N, Grobelsek I, Weingarth D, Presser V. Improved capacitive deionization performance of mixed hydrophobic/hydrophilic activated carbon electrodes. Journal of Physics: Condensed Matter. 2016;28:114003.

[124] Jia BP, Zou LD. Wettability and its influence on graphene nansoheets as electrode material for capacitive deionization. Chemical Physics Letters. 2012;548:23-8.

[125] Duan F, Du X, Li YP, Cao HB, Zhang Y. Desalination stability of capacitive deionization using ordered mesoporous carbon: Effect of oxygen-containing surface groups and pore properties. Desalination. 2015;376:17-24.

[126] Porada S, Schipper F, Aslan M, Antonietti M, Presser V, Fellinger TP. Capacitive deionization using biomass-based microporous salt-templated heteroatom-doped carbons. ChemSusChem. 2015;8:1867-74.

[127] Shao YY, Wang J, Wu H, Liu J, Aksay IA, Lin YH. Graphene based electrochemical sensors and biosensors: A review. Electroanal. 2010;22:1027-36.

[128] Du XA, Guo P, Song HH, Chen XH. Graphene nanosheets as electrode material for electric double-layer capacitors. Electrochimica Acta. 2010;55:4812-9.

[129] Hou CH, Liu NL, Hsi HC. Highly porous activated carbons from resource-recovered Leucaena leucocephala wood as capacitive deionization electrodes. Chemosphere. 2015;141:71-9.

[130] Xu JQ, Zhou K, Chen F, Chen W, Wei XF, Liu XW, et al. Natural integrated carbon architecture for rechargeable lithium-sulfur batteries. ACS Sustainable Chemistry & Engineering. 2016;4:666-70.

[131] Song SJ, Ma FW, Wu G, Ma D, Geng WD, Wan JF. Facile self-templating large scale preparation of biomass-derived 3D hierarchical porous carbon for advanced supercapacitors. Journal of Materials Chemistry A. 2015;3:18154-62.

[132] Hou J, Cao C, Idrees F, Ma X. Hierarchical porous nitrogen-doped carbon nanosheets derived from silk for ultrahigh-capacity battery anodes and supercapacitors. ACS Nano. 2015;9:2556-64.

[133] Chen Z, Wang X, Xue B, Li W, Ding Z, Yang X, et al. Rice husk-based hierarchical porous carbon for high performance supercapacitors: The structure-performance relationship. Carbon. 2020;161:432-44.

[134] Zhao N, Deng L, Luo D, Zhang P. One-step fabrication of biomass-derived hierarchically porous carbon/MnO nanosheets composites for symmetric hybrid supercapacitor. Applied Surface Science. 2020;526:146696.

[135] Yang S, Wang S, Liu X, Li L. Biomass derived interconnected hierarchical micro-meso-macro-porous carbon with ultrahigh capacitance for supercapacitor. Carbon. 2019;147:540-9.

[136] Lin Y, Chen ZY, Yu CY, Zhong WB. Heteroatom-doped sheet-like and hierarchical porous carbon based on natural biomass small molecule peach gum for high-performance supercapacitors. ACS Sustainable Chemistry & Engineering. 2019;7:3389-403.

[137] Hai A, Bharath G, Babu KR, Taher H, Naushad M, Banat F. Date seeds biomass-derived activated carbon for efficient removal of NaCl from saline solution. Process Safety and Environmental Protection. 2019.

[138] Liu G, Qiu L, Deng H, Wang J, Yao L, Deng L. Ultrahigh surface area carbon nanosheets derived from lotus leaf with super capacities for capacitive deionization and dye adsorption. Applied Surface Science. 2020;524:146485.

[139] Liu Y, Zhang X, Gu X, Wu N, Zhang R, Shen Y, et al. One-step turning leather wastes into heteroatom doped carbon aerogel for performance enhanced capacitive deionization. Microporous and Mesoporous Materials. 2020;303:110303.

[140] Huang Y, Yang J, Hu L, Xia D, Zhang Q, Liao Y, et al. Mycelial pellet-derived heteroatom-doped carbon nanosheets with a three-dimensional hierarchical

porous structure for efficient capacitive deionization. Environmental Science: Nano. 2019;6:1430-42.

[141] Zhang XF, Wang B, Yu J, Wu XN, Zang YH, Gao HC, et al. Three-dimensional honeycomb-like porous carbon derived from corncob for the removal of heavy metals from water by capacitive deionization. RSC Advances. 2018;8:1159-67.

[142] Wei HM, Chen J, Fu N, Chen HJ, Lin HL, Han S. Biomass-derived nitrogen-doped porous carbon with superior capacitive performance and high CO_2 capture capacity. Electrochimica Acta. 2018;266:161-9.

[143] Wu L, Liu M, Huo S, Zang X, Xu M, Ni W, et al. Mold-casting prepared free-standing activated carbon electrodes for capacitive deionization. Carbon. 2019;149:627-36.

[144] Liu N-L, Sun S-H, Hou C-H. Studying the electrosorption performance of activated carbon electrodes in batch-mode and single-pass capacitive deionization. Separation and Purification Technology. 2019;215:403-9.

[145] Alencherry T, A.R N, Ghosh S, Daniel J, R V. Effect of increasing electrical conductivity and hydrophilicity on the electrosorption capacity of activated carbon electrodes for capacitive deionization. Desalination. 2017;415:14-9.

[146] Li Y, Xu X, Hou S, Ma J, Lu T, Wang J, et al. Facile dual doping strategy via carbonization of covalent organic frameworks to prepare hierarchically porous carbon spheres for membrane capacitive deionization. Chemical Communications. 2018;54:14009-12.

[147] Baroud TN, Giannelis EP. High salt capacity and high removal rate capacitive deionization enabled by hierarchical porous carbons. Carbon. 2018;139:614-25.

[148] Li Y, Liu Y, Shen J, Qi J, Li J, Sun X, et al. Design of nitrogen-doped cluster-like porous carbons with hierarchical hollow nanoarchitecture and their

enhanced performance in capacitive deionization. Desalination. 2018;430:45-55.

[149] Sun N, Zhang X, Zhao C, Wang H, Lu H, Kang S, et al. Three-Dimensional N-doped Porous Carbon Derived from Monosodium Glutamate for Capacitive Deionization and the Oxygen Reduction Reaction. ChemElectroChem. 2018;5:3873-80.

[150] Huo S, Zhao Y, Zong M, Liang B, Zhang X, Khan IU, et al. Boosting supercapacitor and capacitive deionization performance of hierarchically porous carbon by polar surface and structural engineering. Journal of Materials Chemistry A. 2020;8:2505-17.

[151] Li Y, Hussain I, Qi J, Liu C, Li J, Shen J, et al. N-doped hierarchical porous carbon derived from hypercrosslinked diblock copolymer for capacitive deionization. Separation and Purification Technology. 2016;165:190-8.

[152] Han D-C, Zhang C-M, Guan J, Gai L-H, Yue R-Y, Liu L-N, et al. High-performance capacitive deionization using nitrogen and phosphorus-doped three-dimensional graphene with tunable pore size. Electrochimica Acta. 2020;336:135639.

[153] Krishnamoorthy M, Jha N. Oxygen-Rich Hierarchical Porous Graphene as an Excellent Electrode for Supercapacitors, Aqueous Al-Ion Battery, and Capacitive Deionization. ACS Sustainable Chemistry & Engineering. 2019;7:8475-89.

[154] Liu P, Wang H, Yan T, Zhang J, Shi L, Zhang D. Grafting sulfonic and amine functional groups on 3D graphene for improved capacitive deionization. Journal of Materials Chemistry A. 2016;4:5303-13.

[155] Khan ZU, Yan T, Shi L, Zhang D. Improved capacitive deionization by using 3D intercalated graphene sheet–sphere nanocomposite architectures. Environmental Science: Nano. 2018;5:980-91.

[156] Li Z, Song B, Wu Z, Lin Z, Yao Y, Moon K-S, et al. 3D porous graphene with ultrahigh surface area for microscale capacitive deionization. Nano Energy. 2015;11:711-8.

[157] El-Deen AG, Boom RM, Kim HY, Duan H, Chan-Park MB, Choi J-H. Flexible 3D nanoporous graphene for desalination and bio-decontamination of brackish water via asymmetric capacitive deionization. ACS Applied Materials & Interfaces. 2016;8:25313-25.

Table 1. The preparation methods and porosity characteristics of biochar-based HPC/ EHPC.

No.	Biomass	Carbonization process				Pre-treatment	Activation process				*SSA* ($m^2\ g^{-1}$)	*PV* ($m^3\ g^{-1}$)	R_{meso} (%)	Ref.
		Reactor type	T_c (°C)	HR_c (°C min^{-1})	t_c (h)		Activation method (Activation agent)	T_a (°C)	HR_a (°C min^{-1})	t_a (h)				
1	Shrimp shell (N-doped EHPC)	Pyrolysis	400	5	2	HCl washed impurities	Chemical activation (KOH)	850	5	1	3171	1.93	49.4	[36]
2	Spruce-pine-fir	Pyrolysis	800	5	2	–	Physical activation (Air)	350	–	7	725	0.29	–	[35]
3	Natural basswood	Pyrolysis	1000	–	6	–	Physical activation (CO_2)	750	–	10	839	0.58	23.6	[50]
4	Auricularia (EHPC)	HTC	180	–	12	–	Chemical activation (KOH)	850	5	2	1401	0.90	20.6	[113]
5	Watermelon peel	Pyrolysis	800	5	3	HF washed impurities	Chemical activation ($KHCO_3$)	800	5	3	2360	1.31	–	[111]
6	Loofa sponge	Pyrolysis	600	–	1	–	Chemical activation (KOH)	800	–	1	1819	0.95	18.9	[116]
7	*Leucaena leucocephala* wood	Pyrolysis	400	5	1	–	Physicochemical activation (KOH/CO_2)	800	5	2	1901	1.09	45.2	[129]
8	Kelp	Pyrolysis	700	5	1	HCl washed impurities	Chemical activation (KOH)	800	5	2	2614	1.40	–	[114]

No.	Biomass	Carbonization process				Pre-treatment	Activation process				*SSA* ($m^2\ g^{-1}$)	*PV* ($m^3\ g^{-1}$)	R_{meso} (%)	Ref.
		Reactor type	T_c (°C)	HR_c (°C min^{-1})	t_c (h)		Activation method (Activation agent)	T_a (°C)	HR_a (°C min^{-1})	t_a (h)				
9	Rice husk (EPHC)	Pyrolysis	900	–	1	HF leached SiO_2 template	Physical activation (N_2/steam)	850	–	0.5	861	0.35	–	[64]
10	Rice husk (EPHC)	HTC	230	–	48	NH_4HF_2 leached SiO_2 template	Higher pyrolysis	900	5	–	525	0.49	76.4	[26]
11	Rice husk (EPHC)	Pyrolysis	700	2	2	HCl leached SiO_2 template	Chemical activation (EtOH)	800	1	2	78.5	0.21	–	[30]
12	The bark of plane trees (S-doped-EHPC)	Pyrolysis	750	–	5	HCl washed impurities	–	–	–	–	528	0.72	–	[130]
13	Oyster shell + soft pitch (EHPC)	Pyrolysis	900	5	5	HCl leached CaO template	–	–	–	–	1258	0.58	69.6	[27]
14	Soybean hulls (S-doped-EHPC)	Pyrolysis	800	3	2	HCl washed impurities	Chemical activation (KOH)	700	3	2	1232	0.54	–	[18]
15	Porphyra (N- doped EHPC)	Pyrolysis	300 (+800)	–	1 (+2)	HNO_3 leached Ni particle template	Physical activation (Steam)	800	–	1	811	–	–	[65]
16	Rice husk (MnO_2-modified EHPC)	Pyrolysis	500	–	1	NaOH leached SiO_2 template	Chemical activation (KOH)	700	–	2	1751	1.11	55.9	[13]

No.	Biomass	Carbonization process				Pre-treatment	Activation process				*SSA* ($m^2\ g^{-1}$)	*PV* ($m^3\ g^{-1}$)	R_{meso} (%)	Ref.
		Reactor type	T_c (°C)	HR_c (°C min^{-1})	t_c (h)		Activation method (Activation agent)	T_a (°C)	HR_a (°C min^{-1})	t_a (h)				
17	Rice husk (EHPC)	Pyrolysis	500	–	1	NaOH leached SiO_2 template	Chemical activation (KOH)	700	–	1	2804	1.80	–	[67]
18	*Indicalamus* leaf (EHPC)	Pyrolysis	900	5	4	HF leached metal-organic complexes template	–	–	–	–	1801	1.45	–	[99]
19	*Enteromorpha prolifera*	Pyrolysis	500	15	1.5	–	Chemical activation (KOH)	750	15	1	3332	2.46	60.4	[68]
20	Artemia cyst shell (O-doped EHPC)	Pyrolysis	300 (+700)	1	3 (+4)	HNO_3 washed impurities	Chemical activation (KOH)	700	10	1	1758	0.76	28.9	[100]
21	Corn husk	–	–	–	–	–	Chemical activation (KOH)	800	5	1	928	0.53	26.4	[131]
22	Soybean root	Pyrolysis	500	5	2	–	Chemical activation (KOH)	800	5	2	2143	0.94	13.8	[85]
23	Silk (N-doped EHPC)	–	–	–	–	–	Chemical activation ($ZnCl_2$)	900	2	1	2494	2.28	79.8	[132]
24	Peanut shell	HTC	180	–	48	H_2SO_4 washed impurities	Chemical activation (KOH)	800	–	1	2396	1.31	35.5	[86]
25	Sugar cane bagasse (N-doped EHPC)	–	–	–	–	–	Chemical activation ($CaCl_2$ as green activation agent)	800	5	2	946	1.39	17.7	[74]

No.	Biomass	Carbonization process				Pre-treatment	Activation process				*SSA* ($m^2\ g^{-1}$)	*PV* ($m^3\ g^{-1}$)	R_{meso} (%)	Ref.
		Reactor type	T_c (°C)	HR_c (°C min^{-1})	t_c (h)		Activation method (Activation agent)	T_a (°C)	HR_a (°C min^{-1})	t_a (h)				
26	Silkworm cocoon (N-doped EHPC)	Pyrolysis	450	5	0.5	–	Chemical activation (KOH)	900	1	2	3386	2.20	45.5	[28]
27	Soybean milk (N-doped EHPC)	–	–	–	–	HCl leached $CaCO_3$ template	Chemical activation (KOH)	700	3	2	1208	0.7	42.9	[66]
28	Kraft lignin (O-N-S co-doped EHPPC)	Pyrolysis	400	2	1	–	Higher pyrolysis	800	4	1	1307	0.67	–	[23]
29	Barley (N-S co-doped EHPC)	–	–	–	–	–	Chemical activation (copper citrate)	800	5	2	2140	1.16	56.0	[19]
30	Peanut shell (N-doped EHPC)	HTC	200	–	4	–	Physicochemical activation (KOH/CO_2)	800	10	1.5	1029	1.38	72.5	[101]
31	Rice husk (EHPC)	Pyrolysis	600	–	1	NaOH leached SiO_2 template	Chemical activation (NaOH)	750	–	1	1789	1.15	37.4	[133]
32	Wood powders (N-doped EHPC)	–	–	–	–	–	Orange peel as green activation agent	800	5	2	282	0.31	71.0	[75]
33	Fishbone (N-doped EHPC)	Pyrolysis	850	5	2	HCl leached $Ca_{10}(PO4)_6(OH)_2$ template	–	–	–	–	1337	0.85	62.4	[76]

No.	Biomass	Carbonization process				Pre-treatment	Activation process				*SSA* ($m^2\ g^{-1}$)	*PV* ($m^3\ g^{-1}$)	R_{meso} (%)	Ref.
		Reactor type	T_c (°C)	HR_c (°C min^{-1})	t_c (h)		Activation method (Activation agent)	T_a (°C)	HR_a (°C min^{-1})	t_a (h)				
34	Litchi shell (MnO-modified EHPC)	–	–	–	–	–	Chemical activation (KOH)	800	–	2	1123	–	–	[134]
35	Mixed crab shell and rice husk (EHPC)	HTC	200	–	3	NaOH leached $CaCO_3$ and SiO_2 template	Chemical activation (KOH)	700	5	3	3557	2.02	48.5	[96]

Carbonization temperature: T_c; carbonization heating rate: HR_c; carbonization time: t_c; activation temperature: T_a; activation heating rate: HR_a; activation time: t_a; specific surface area: *SSA;* total pore volume: *PV;* mesoporosity: $R_{meso}=V_{meso}/PV$, mesopore volume: V_{meso}

Table 2. Application of biochar-based HPC/EHPC for SCs.

No.	Biomass	Test system/ Electrolyte	Current density ($A\ g^{-1}$)	Specific capacitance ($F\ g^{-1}$)	Energy density ($Wh\ kg^{-1}$)	Power density ($W\ kg^{-1}$)	Capacity retention rate	Ref.
1	Rice husk (MnO_2-modified EHPC)	3E/0.5 M Na_2SO_4	5	210	–	–	80.2% after 5000 cycles at 5 $A\ g^{-1}$	[13]
2	*Indicalamus* leaf	2E/1 M Na_2SO_4	0.5	326	17.3 23.7	4355 224.5	98% after 8000 cycles at 5 $A\ g^{-1}$	[99]
3	Soybean root	2E/EMIMBF4	0.5	276	40.7 100.5	63000 4353	98% after 10000 cycles at 5 $A\ g^{-1}$	[85]
4	Silk (N-doped EHPC)	2E/EMIMBF4	0.1	242	52.5 102	8750 875	92% after 10000 cycles at 2 $A\ g^{-1}$	[132]
5	Peanut shell	2E/1 M $NaClO_4$	0.1	161	50 285	16500 201	88% after 100000 cycles at 51.2 $A\ g^{-1}$	[86]
6	Silkworm cocoon (N-doped EHPC)	2E/1M $MIMBF_4$	0.5	263.5	27.95 34.4	23910 3120	82.8% after 3000 cycles at 10 $A\ g^{-1}$	[28]
7	Soybean milk (N-doped EHPC)	3E/6 M KOH/ PVA gel	0.5	149.3	8.2 10.2	19600 351	89.3% after 5000 cycles at 0.5 $A\ g^{-1}$	[66]
8	Shaddock endotheliums (O-N-S co-doped EHPC)	3E/1 M $EMIMBF_4$/AN	0.2	550	29.25 46.88	4500 300	93.7% after 10000 cycles at 5 $A\ g^{-1}$	[135]
9	Crab ($CoFe_2O_4$-modified EHPC)	3E/6M KOH	1	701.8	18.2 22.3	4992 497	90.9% after 10000 cycles at 1 $A\ g^{-1}$	[25]

No.	Biomass	Test system/ Electrolyte	Current density (A g^{-1})	Specific capacitance (F g^{-1})	Energy density (Wh kg^{-1})	Power density (W kg^{-1})	Capacity retention rate	Ref.
10	Peach gum (O-N co-doped EHPC)	3E/1 M Na_2SO_4	0.2	406	15.97 25.56	20000 500	91.76% after 7000 cycles	[136]
11	Mixed crab shell and rice husk (EHPC)	2E/1 M Na_2SO_4	0.5	474	20.3 30.5	9000 225	95.6% a after 20000 cycles	[29]
12	Kraft lignin (O-N-S co-doped EHPPC)	3E/6 M KOH	0.2	244.5	32.2 66.8	40000 1750	91.6% over 10000 cycles	[23]
13	Rape pollen (N-S co-doped EHPPC)	2E/1 M Na_2SO_4	1	361.6	10.7 32.2	4100 89	94.5% after 20000 cycles at 5 A g^{-1}	[102]
14	Ant powder (O-N-S co-doped EHPC)	2E/1 M $EMIMBF_4$	0.1	352	67 107	18000 900	5% loss over 10000 cycle	[87]
15	Chicken bone (MnO_2-modified EHPC)	2E/1 M Na_2SO4	2.0	217.3	11.5 60.8	20700 1400	95% after 10000 cycles	[24]
16	Barley (N-S co-doped EHPC)	3E/1 M Na_2SO4 (3E/6 M KOH)	0.5 (0.5)	56.8 (401.6)	30.9 16.9	500 8245	97.9% after 20000 cycles at 5 A g^{-1}	[19]
17	Peanut shell (N-doped EHPC)	3E/6 M KOH	0.5	310.6	25.31 40.92	17195 990	90.14% after 5000 cycles at 2 A g^{-1}	[101]
18	Rice husk (EHPC)	3E/6 M KOH	0.5	263	7.6 ~6.5	~4000 243	99.6% after 20 000 cycles at 1 A g^{-1}	[133]
19	Litchi shell (MnO-modified EHPC)	3E/6 M KOH	0.5	795.5	57.7 12.1	400 37775	93.5% after 5000 cycles at 2 A g^{-1}	[134]

Table 3. Application of biochar-based HPC/EHPC for CDI.

No.	Biomass	Scan rate (mV s^{-1})	Specific capacitance (F g^{-1})	Voltage	Pollutant	Initial concentration (mg L^{-1})	Flow rate (mL min^{-1})	Electrosorption capacity (mg g^{-1})	Ref.
1	Natural basswood	10	87	1.2	NaCl	100	20	5.7	[50]
2	Loofa sponge	5	93	1	NaCl	854.4	5	22.5	[116]
3	Auricularia	10	73	1.2	NaCl	55.7	–	7.7	[113]
4	Rice husk	0	60	1.5	NaCl	100	20	17.7	[64]
5	Watermelon peel	1	224	1.2	NaCl	500	40	17.4	[111]
6	Kelp	5	190	1.2	NaCl	500	20	27.2	[114]
7	Eggplant	–	–	–	NaCl	–	–	31.9	[112]
8	Date seeds	10	400	1.2	NaCl	250	10	22.2	[137]
9	Lotus leaf	–	–	1.6	NaCl	2000	15	65.0	[138]

No.	Biomass	Scan rate ($mV\ s^{-1}$)	Specific capacitance ($F\ g^{-1}$)	Voltage	Pollutant	Initial concentration ($mg\ L^{-1}$)	Flow rate ($mL\ min^{-1}$)	Electrosorption capacity ($mg\ g^{-1}$)	Ref.
10	Leather wastes (N-O-S codoped EHPC)	2	132	1.2	NaCl	500	10	20.9	[139]
11	Egg whites (N-doped EHPC)	5	137	1.2	NaCl	500	10	26.7	[120]
12	Mycelial pellet (N-S codoped EHPC)	10	47	1.2	NaCl	500	10	18.7	[140]
13	Tamarind shell (N-dope EHPC)	10	175	1.2	NaCl	600	10	18.8	[121]
14	Rice husk (EHPC)	5	121	1.2	NH_4^+	10.7	7.5	1.53	[115]
15	Rice husk husk (EHPC)	5	121	1.2	Mg^{2+}	47.6	7.5	1.54	[115]
16	Rice husk husk (EHPC)	5	121	1.2	Cu^{2+}	13.4	7.5	0.52	[115]
17	Corncob	1	452	1	Cr(VI)	30	–	82.4	[141]

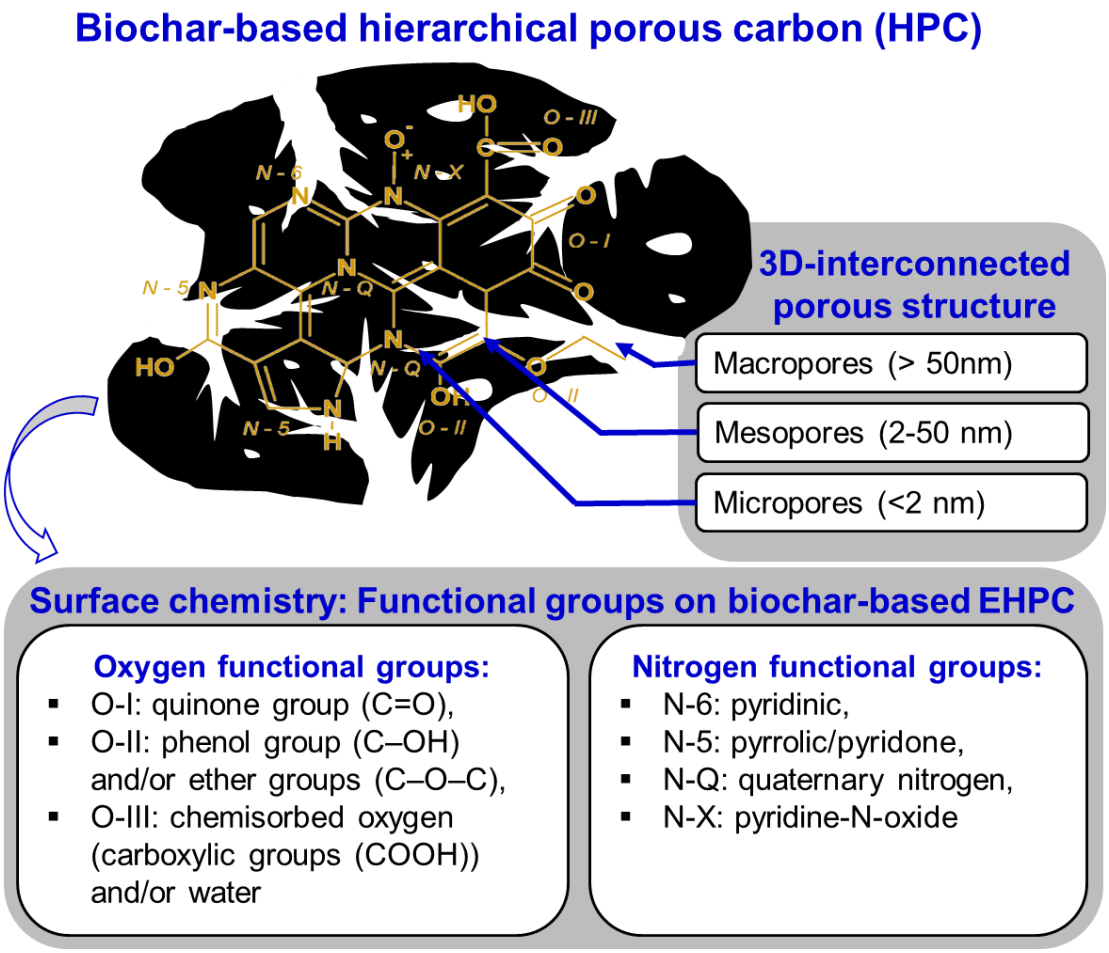

Fig. 1. Schematic model of the porosity structure and surface chemistry of biochar-based HPC/EHPC. Information regarding the functional groups was adopted from Jurcakova et al. [20]. Nitrogen functional groups present in the N-doped biochar-based HPC or EHPC.

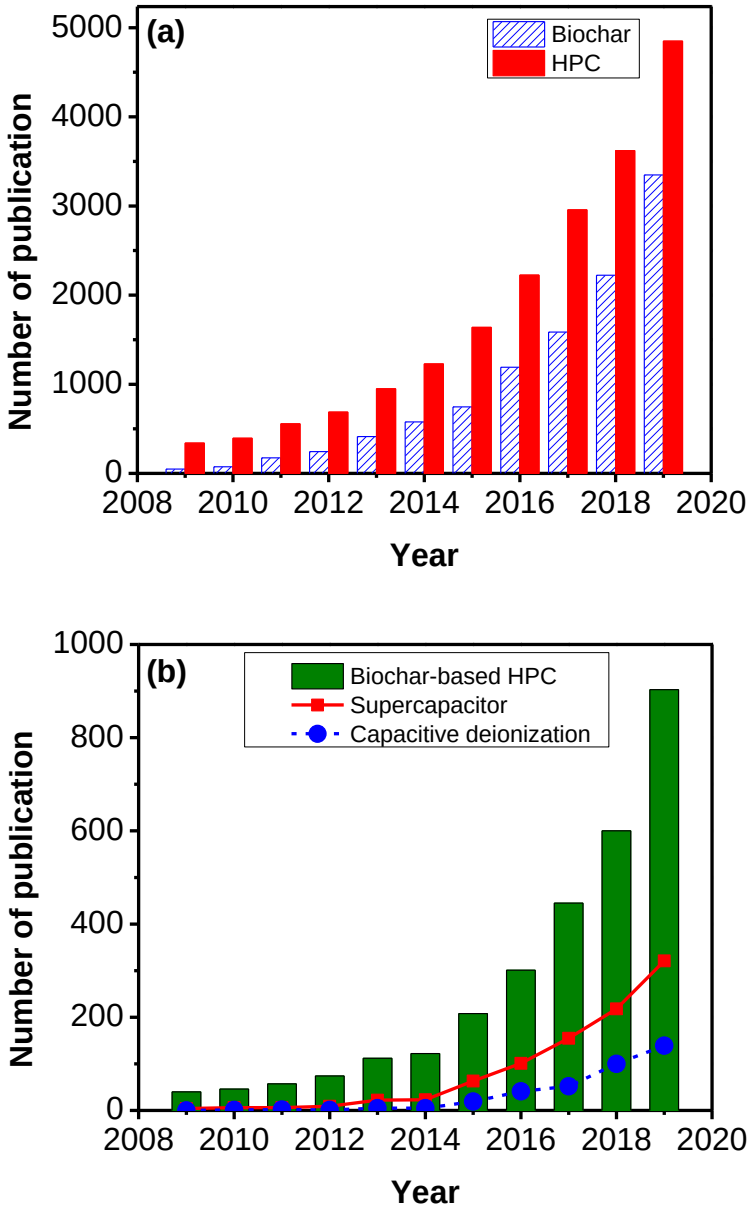

Fig. 2. The number of publications related to (a) HPC and biochar-based HPC/EHPC, and (b) utilization of biochar-based HPC/EHPC for electrosorption and energy storage during the years from 2009 to 2019 (according to ISI Web of Science™).

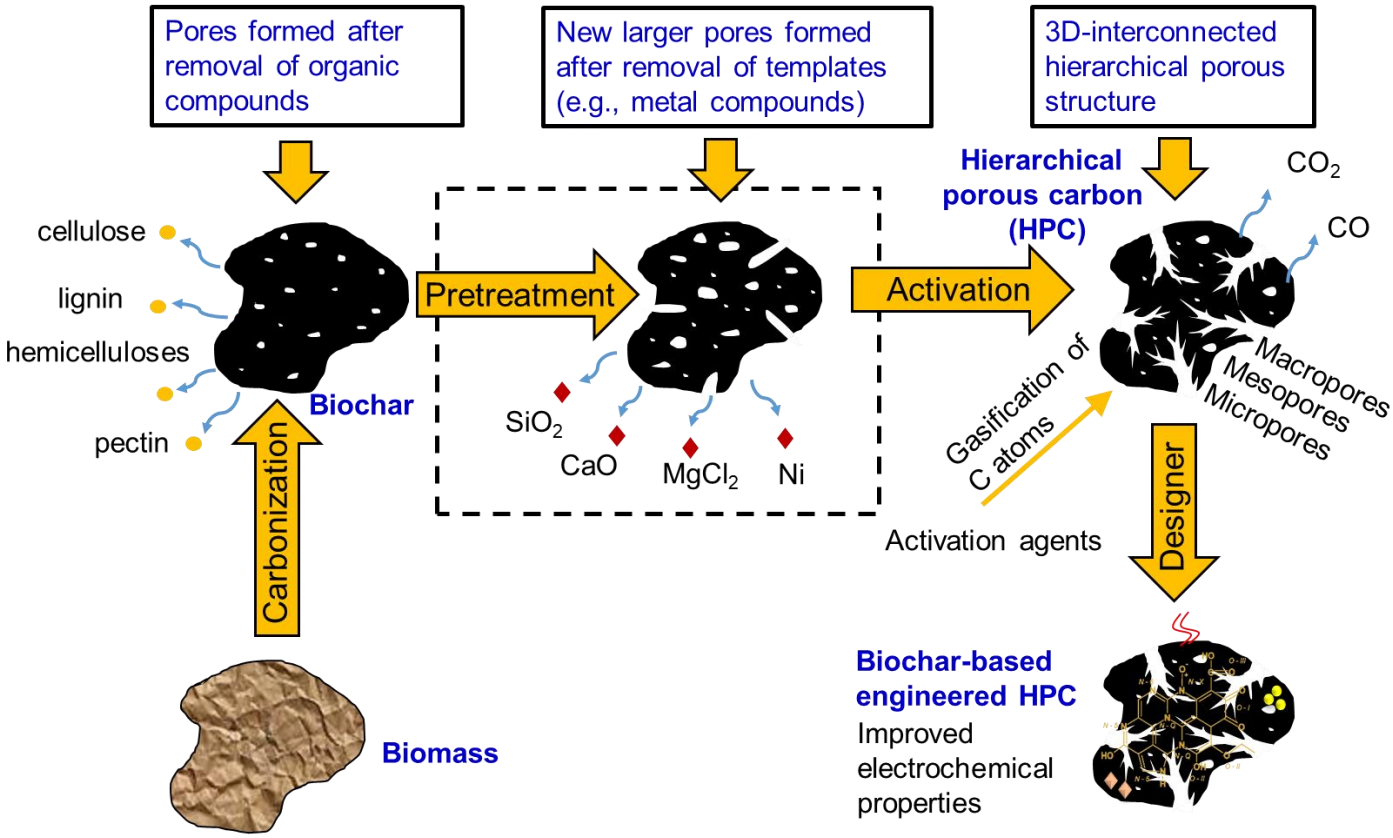

Fig. 3. Illustration of the mechanism for pore development of biochar-based HPC and EHPC, the dotted line is presented for an optional step.

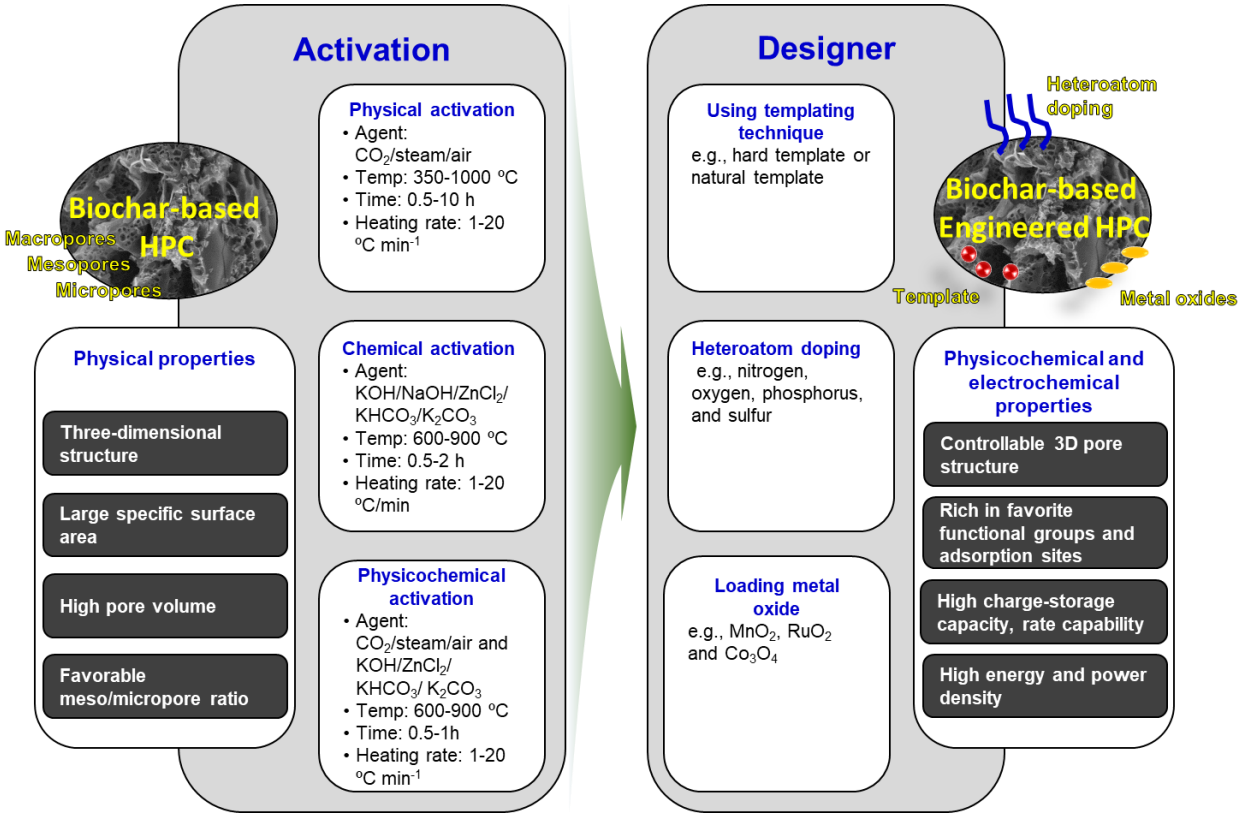

Fig. 4. Activation methods to produce biochar-based HPC and the design of biochar-based EHPC.

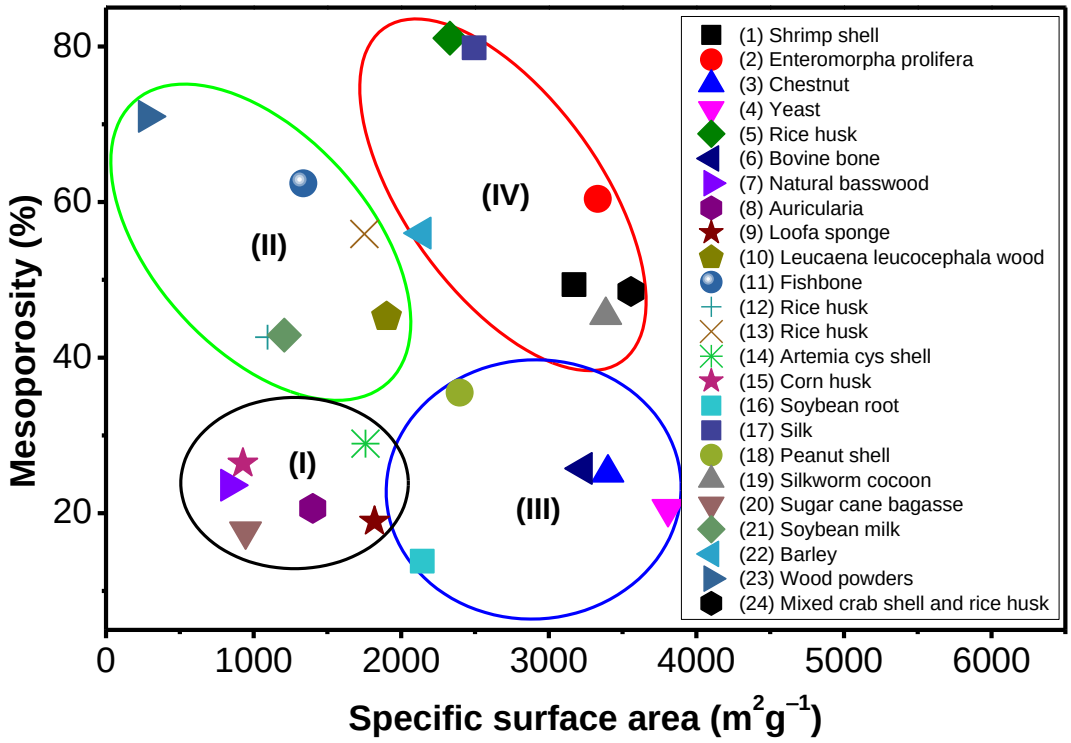

Fig. 5. The SSA and mesoporosity of biochar-based HPC/EHPC-derived from different biomass: (1) Shrimp shell [36], (2) *Enteromorpha prolifera* [68], (3) chestnut [142], (4) yeast [60], (5) rice husk [17], (6) bovine bone [37], (7) natural basswood [50], (8) auricularia [113], (9) loofa sponge [116], (10) *Leucaena leucocephala* wood [129], (11) fishbone [76], (12) rice husk [14], (13) rice husk [13], (14) *Artemia* cyst shells [100], (15) corn husk [131], (16) soybean root [85], (17) silk [132], (18) peanut shell [86], (19) silkworm cocoon [28], (20) sugar cane bagasse [74], (21) soybean milk [66], (22) barley [19], (23) wood powders [75] and (24) mixed crab shell and rice husk [96]. Group I (black elip): SSA < 2000 m^2 g^{-1} and mesoporosity <40%; Group II (green elip): SSA < 2000 m^2 g^{-1} and mesoporosity >40%; Group III (blue elip): SSA > 2000 m^2 g^{-1} and mesoporosity <40%; Group IV (red elip): SSA > 2000 m^2 g^{-1} and mesoporosity >40%.

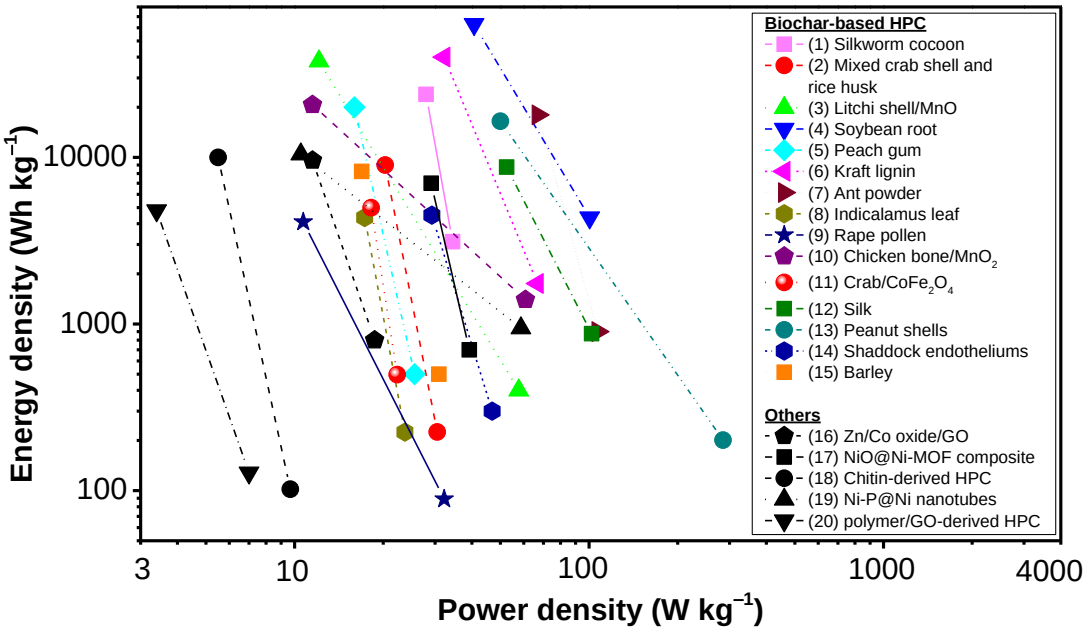

Fig. 6. Comparisons of the electrochemical performance of SCs assembled from HPCs/EHPCs derived from different biomass/biochars: (1) silkworm cocoon [28], (2) mixed crab shell and rice husk [29], (3) litchi shell [66], (4) soybean root [85], (5) peach gum [136], (6) kraft lignin [23], (7) ant powder [87], (8) *Indicalamus* leaf [99], (9) rape pollen [102], (10) chicken bone [24], (11) crab [25], (12) sink [132], (13) peanut shell [86], (14) shaddock endotheliums [136], (15) barley [19] and other commercial precursor-derived materials: (16) ZIF-derived graphene-based 2D Zn/Co oxide hybrid [88], (17) NiO derived NiO@Ni-MOF composite [89], (18) heteroatoms-doped HPC derived from chitin [90], (19) ultrafine Ni–P@Ni nanotubes [91], (20) HPC nanosheets derived from polymer/graphene oxide (GO) hydrogels [92]. Two points regarding each material present the highest and lowest energy density at the lowest and highest power density, respectively.

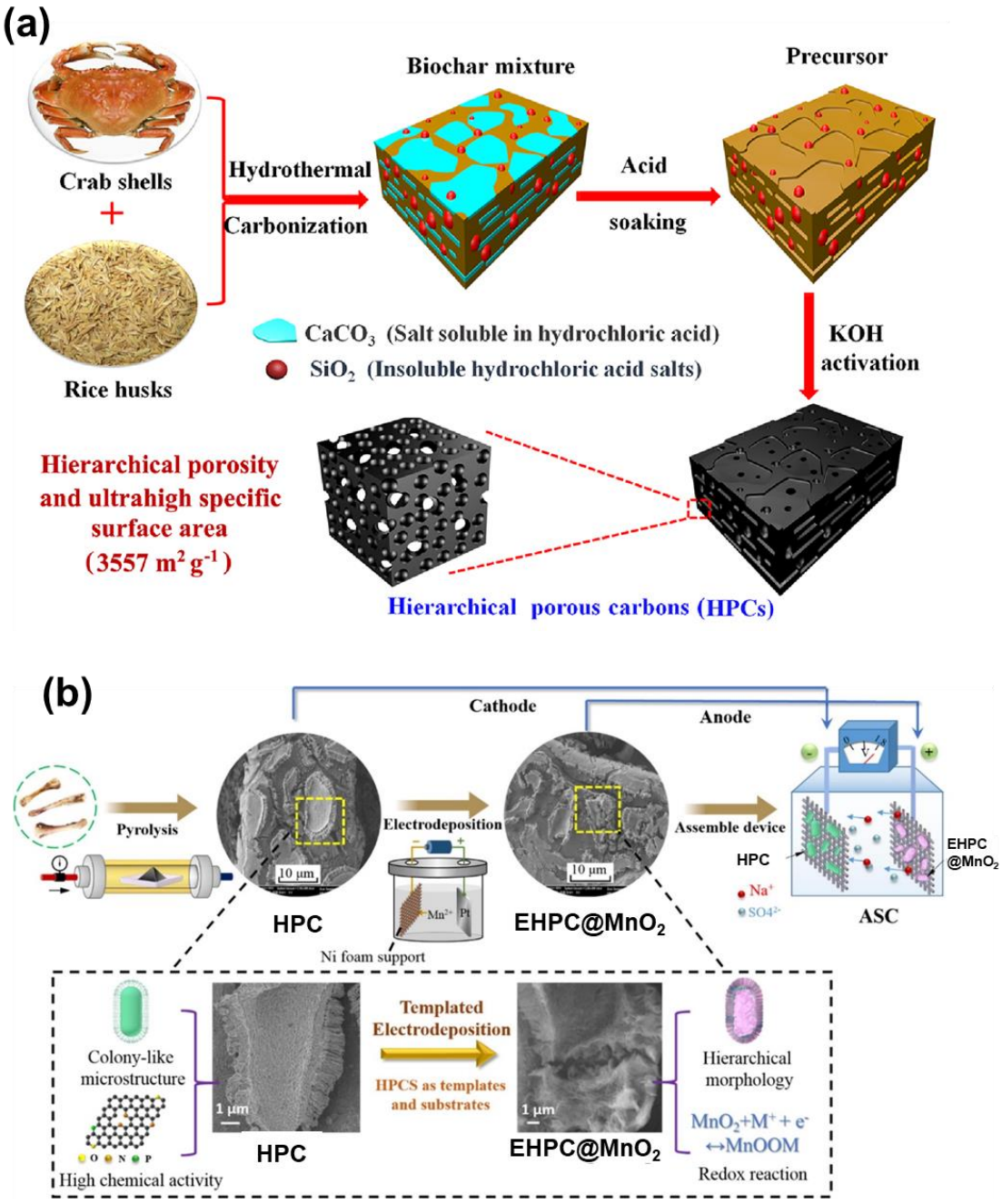

Fig. 7. (a) Schematic illustration of the preparation steps for mixed crab shell and rice husk biochar-based EHPC, (b) Chicken bones-based HPC and EHPC@MnO_2 composite electrodes preparation procedure for SCs. Reproduced with permission from Ref. [96] and [24].

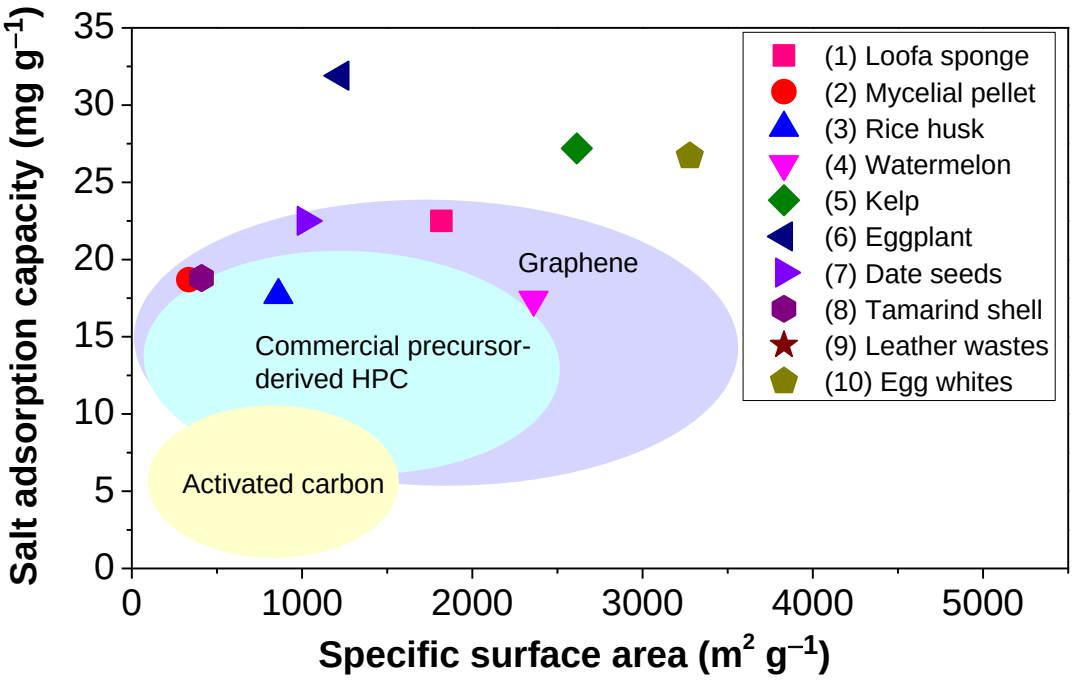

Fig. 8. Comparison of salt adsorption capacities of HPCs/EHPCs derived from different biomass (1) loofa sponge [116], (2) mycelial pellet [140], (3) rice husk [64], (4) watermelon peel [111], (5) kelp [114], (6) eggplant [112], (7) date seeds [137], (8) Tamarind shell [121], (9) leather wastes [139], (10) egg whites [120] with other materials, i.e., activated carbon [115, 143-145], commercial precursor-based HPC [146-151], and graphene [152-157].

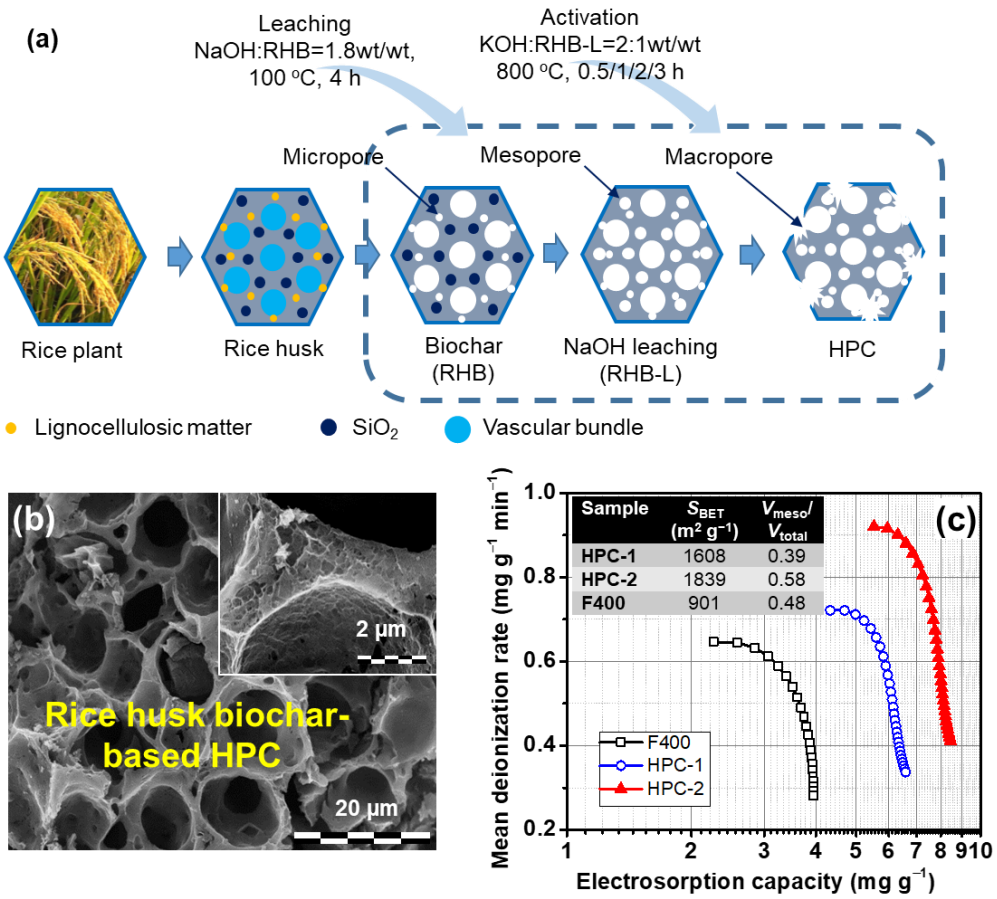

Fig. 9. Applications of rice husk biochar-based EHPC for electrosorption application (a) fabrication process of HPC, (b) SEM images and (c) CDI Ragone plots and eggplant biochar-based HPC Ref. [115].